

# Optimisation of an In Vitro Macrophage Model to Investigate the Interactions with Adipose Tissue-derived Stromal Cells and Extracellular Matrix

---



LAURA LYKKE LETHAGER  
MEDICINE WITH INDUSTRIAL SPECIALISATION,  
MASTER THESIS IN BIOMEDICINE,  
AALBORG UNIVERSITY, 2023



AALBORG UNIVERSITET  
STUDENTERRAPPORT

Cardiology  
**Stem Cell**  
Centre

Department of Health Science and Technology  
Medicine with Industrial Specialisation  
Selma Lagerlöfs Vej 249  
9260 Gistrup  
<http://www.hst.aau.dk>

**Title:**

Optimisation of an In Vitro Macrophage Model to Investigate the Interactions with Adipose Tissue-derived Stromal Cells and Extracellular Matrix

**Dansk Titel:**

Optimering af en in vitro makrofag model med henblik på at undersøge interaktionerne med fedtvævs-deriverede stromale celler og ekstracellulær matrix

**Project:**

Master Thesis, 9<sup>th</sup> and 10<sup>th</sup> semester, Biomedicine  
Medicine with Industrial Specialization, Aalborg University

**Project period:**

September 2022 to June 2023

**Project group, participants, and study number:**

Group 9025  
Laura Lykke Lethager, 20185283

**Internal Supervisor:**

Simone Riis Porsborg

**External Supervisor:**

Morten Juhl Nørgaard

**Frontpage:** TGF- $\beta$  stimulated normal human dermal fibroblasts at crowded conditions. Stained with Sirius red (0.1%) in Picric Acid.

**Number of Pages:** 61

**Number of Appendices:** 10

# 1 | Preface

This thesis is written in collaboration with Cardiology Stem Cell Center. It composes a tool, and is intended for use in future research, with the aim of developing potency assays for a cellular therapy product based on adipose-derived stromal cells.

In anticipation of this, comprehensive details are included to ensure that the contents are sufficient to reproduce and refine any future experiments.

## 2 | Acknowledgements

This thesis has been written in collaboration with Cardiology Stem Cell Center with kind and committed supervision from Simone Riis Porsborg and Morten Juhl Nørgaard. I am very grateful for all of your help and your great advice along the way.

A special thanks to everyone at the Cardiology Stem Cell Center for your support in the past year, especially to Rebekka Harary Søndergaard for always making time to help me when needed.

The macrophage-ASC-coculture model was developed in collaboration with Kian Haseli, thank you for all the fun hours working in the lab.

## 3 | Resumé

**Formål:** I de senere år stromale celler fra fedtvæv (ASCer) blevet undersøgt som celleterapi på grund af deres immunmodulatoriske egenskaber, og fordi de kan regulere funktionen af immunceller, såsom makrofager. Makrofager er plastiske celler med både pro- og anti-inflammatoriske funktioner. Disse egenskaber gør ASCerne i stand til at mindske inflammation og forebygge fibrose. Fibrose kan opstå som følge af vedvarende inflammation og medfører nedsat funktionalitet af vævet. ASCer kan interagere med de omkringliggende celler gennem både parakrine udskillelser af for eksempel proteiner og ved celle-celle kontakt. Den præcise virkningsmekanisme bag interaktionen mellem ASCer og makrofager er dog stadig ukendt. Derfor var formålet med dette studie at undersøge effekten af ASCer på makrofagernes fibrotiske effekt.

**Metoder:** For at udvikle en makrofag-ASC-kokultur model blev den optimale koncentration af lipopolysakkarid og interferon- $\gamma$  bestemt ved at måle koncentrationen af tumor necrosis factor- $\alpha$ , som blev udskilt af makrofagerne. Derefter blev makrofager isoleret fra ASCerne ved hjælp af Dynabeads med CD90 antistof og herefter sået ud i en extracellulær matrix, som var dannet af transforming growth factor- $\beta$ -stimulerede fibroblaster. Efter seks dage blev niveauerne af collagen I og III bestemt som et mål for udskillelsen af ekstracellulær matrix. Optimering af fibroblasternes optimale densitet fik dem til at danne en tæt ekstracellulær matrix, hvilket blev bestemt ved farvning med Sirius Rød (0,1%) i pikrinsyre.

**Resultater og konklusion:** Der blev etableret en makrofag-ASC-kokultur model, hvor makrofagerne blev aktiveret med 100 ng/mL lipopolysakkarid og 20 ng/mL interferon- $\gamma$ . Efter seks dage i kokultur med fibroblaster havde de ASC-behandlede makrofager forårsaget signifikant nedsatte niveauer af kollagen I og kollagen III, hvilket tyder på, at makrofagerne er i stand til at påvirke udskillelsen af ekstracellulær matrix. Den optimale koncentration af makrofager var 6250 M1/cm<sup>2</sup>, idet denne koncentration resulterede i den største signifikante og numeriske forskel mellem de ASC-behandlede makrofager og en kontrol med aktiverede makrofager.

## 4 | Abstract

**Aim:** In recent years, adipose-derived stromal cells (ASCs) have been investigated for use as a cellular therapy, due to their immunomodulatory properties and their ability to regulate the function of immune cells, such as macrophages. Macrophages are plastic cells with both pro- and anti-inflammatory functions. These features enable them to reduce inflammation and prevent fibrosis. Fibrosis can arise as a result of prolonged inflammation and this leads to decreased tissue functionality. The ASCs can interact with the surrounding cells through both paracrine secretion and cell-cell contact. However, the exact mechanisms of action for the interactions between ASCs and macrophages are still unknown. Therefore, the aim of this study was to investigate the effect of ASCs on the fibrotic effects of macrophages.

**Methods:** To develop a macrophage-ASC-coculture, the optimal concentration of activating stimuli, lipopolysaccharide and interferon- $\gamma$ , was determined by measuring the concentration of secreted tumor necrosis factor- $\alpha$  by the macrophages. Hereafter, macrophages were isolated from the ASCs using Dynabeads coated with CD90 antibody, and then seeded onto an extracellular matrix derived from transforming growth factor- $\beta$ -stimulated fibroblasts. After six days, the levels of collagen I and III were determined as a measure of deposition of extracellular matrix. Optimisation of fibroblast seeding density allowed them to create a dense extracellular matrix, which was determined through staining with Sirius Red (0.1%) in Picric Acid.

**Results and Conclusion:** A macrophage-ASC-coculture model was established, and the optimal concentrations of lipopolysaccharide and interferon- $\gamma$  were found to be 100 ng/mL and 20 ng/mL, respectively. After six days of coculture with fibroblasts, the ASC-treated macrophages had resulted in significantly decreased levels of collagen I and III, which suggests that macrophages are able to affect the deposition of extracellular matrix. The optimal seeding density of the macrophages was 6250 M1/cm<sup>2</sup> at which concentration the greatest significant and numerical difference between the ASC-treated macrophages and the mature macrophages was found.

# Contents

<b>1</b>	<b>Preface</b>	<b>3</b>
<b>2</b>	<b>Acknowledgements</b>	<b>4</b>
<b>3</b>	<b>Resumé</b>	<b>5</b>
<b>4</b>	<b>Abstract</b>	<b>6</b>
<b>5</b>	<b>Abbreviations</b>	<b>9</b>
<b>6</b>	<b>Introduction</b>	<b>10</b>
6.1	Anti-Fibrotic Effects of Adipose-Stromal Cells . . . . .	11
6.2	Macrophages . . . . .	14
6.3	Aim of Study . . . . .	18
<b>7</b>	<b>Methods</b>	<b>19</b>
7.1	Cryopreservation of Peripheral Blood Mononuclear Cells . . . . .	21
7.2	Isolation of Monocytes and Generation of Macrophages . . . . .	21
7.3	Coculture of Macrophages and ASCs . . . . .	22
7.4	Validation of the Macrophage Model . . . . .	23
7.5	Separation of the Coculture . . . . .	25
7.6	Evaluating the effect of ASC-treated Macrophages on the Extracellular Matrix	26
7.7	Microscopy . . . . .	27
7.8	Flow Cytometry . . . . .	28
7.9	Statistics . . . . .	29
<b>8</b>	<b>Results</b>	<b>30</b>
8.1	Validation of the Macrophage Model . . . . .	30
8.2	Separation of Coculture . . . . .	31
8.3	Determining the Optimal Seeding Density of Fibroblasts . . . . .	33
8.4	Initial Setup of Macrophage and Fibroblast Coculture . . . . .	35
8.5	Determining Optimal Seeding Density of Macrophages in an Extended Setup	37

<b>9 Discussion</b>	<b>42</b>
9.1 Conclusion . . . . .	47
<b>10 Bibliography</b>	<b>48</b>
<b>A Appendix</b>	<b>52</b>
A.1 Table of Macrophage Markers . . . . .	52
A.2 Dilution of Samples for ELISA . . . . .	53
A.3 Determination of Optimal Concentrations of Activating Stimuli . . . . .	54
A.4 Channels in Fluorescent Microscopy . . . . .	55
A.5 Optimization of PKH26 Concentration . . . . .	56
A.6 Flowcytometric Analysis using CD45 and CD90 . . . . .	57
A.7 Titration of Dynabeads . . . . .	58
A.8 Aggregation in a Single Cell Suspension . . . . .	59
A.9 Macrophage Viability . . . . .	60
A.10 PicroSirius Staining of Macrophages . . . . .	61

## 5 | Abbreviations

<b>A</b>	acceleration	<b>mM1</b>	mature M1
<b>ASC</b>	adipose-derived stromal cell	<b>mM2</b>	mature M2
<b>ASC-M1</b>	ASC-treated M1	<b>MMC</b>	macromolecular crowding
<b>BSA</b>	bovine serum albumine	<b>MMP</b>	matrix metalloproteinase
<b>CXCL</b>	C-X-C motif chemokine ligand	<b>MSC</b>	mesenchymal stromal cell
<b>D</b>	deceleration	<b>NHDF</b>	normal human dermal fibroblasts
<b>DAMP</b>	damage-associated molecular pattern	<b>PAMP</b>	pathogen-associated molecular pattern
<b>DMEM</b>	Dulbecco's modified eagle medium	<b>PBMC</b>	peripheral blood mononuclear cell
<b>DMSO</b>	dimethyl sulfoxide	<b>Pen/Strep</b>	Penicillin-Streptomycin
<b>ECM</b>	extracellular matrix	<b>PicroSirius</b>	Sirius Red (0.1%) in Picric Acid
<b>EDTA</b>	ethylenediaminetetraacetic acid	<b>RGD</b>	arginine-glycine-aspartic acid
<b>ELISA</b>	enzyme-linked immunosorbent assay	<b>RT</b>	room temperature
<b>FACS</b>	fluorescence-activated cell sorting	<b>TGF</b>	transforming growth factor
<b>FBS</b>	fetal bovine serum	<b>Th1</b>	type 1 T helper
<b>GM-CSF</b>	granulocyte macrophage colony stimulating factor	<b>Th2</b>	type 2 T helper
<b>HCL</b>	hydrochloric acid	<b>TIMP</b>	tissue inhibitor of metalloproteinase
<b>HLA</b>	human leukocyte antigen	<b>TNF</b>	tumor necrosis factor
<b>ICC</b>	immunocytochemistry	<b>qPCR</b>	quantitative Polymerase Chain Reaction
<b>IFN</b>	interferon		
<b>IL</b>	interleukin		
<b>imM1</b>	immature M1		
<b>LPS</b>	lipopolysaccharide		
<b>M1:ASC</b>	macrophage and ASC		
<b>M1:NHDF</b>	macrophage and fibroblast		
<b>MACS</b>	magnetic-activated cell sorting		
<b>M-CSF</b>	macrophage colony stimulating factor		
<b>MFI</b>	median fluorescence intensity		

## 6 | Introduction

In the past decade, cell-based therapies have been investigated for use in the repair and regeneration of damaged tissue. Most human cells have limited potential for differentiation and thus limited use in tissue regeneration, and it has been a challenge to procure a reliable source of suitable cells (Gimble and Guilak, 2003; Bourin et al., 2013). Recently, cellular therapy products have been suggested for clinical evaluation and market authorization (Bravery et al., 2013). When developing a cellular therapy product, the first step is to characterize the product by identifying relevant biological functions and defining the quality of the product. This is important, because if the quality of the product is not consistent, neither is the clinical effect (Bravery et al., 2013). A way to ensure consistent quality of the product is through potency assays. Potency assays are tests that during product development have been demonstrated to confirm the presence of relevant biological functions of the cellular therapy product. Ideally, potency assays are correlated to product efficacy. Potency assays are based on the initial characterization of the cellular therapy product, and are important tools for managing any process changes and evaluating the product prior to market release. A theory of the mechanism of action of the product must be developed before designing a potency assay, and this should be based on scientific data and reflect the therapeutic rationale for administering the product (Bravery et al., 2013).

An example of a cell type that has been explored for use as a cellular therapy product is the mesenchymal stromal cell (MSC), which meets many of requirements to be a reliable cell source. MSCs can be isolated from various tissues, including adipose tissue and bone marrow, which gives rise to the adipose-derived stromal cell (ASC) and the bone marrow-derived MSC, respectively. MSCs are defined by a set of minimal criteria, stating they must be plastic-adherent when maintained in culture, and express positive markers CD105, CD73, and CD90 while lacking expression of negative markers CD45, CD34, CD14 or CD11b, CD79 $\alpha$  or CD19, and human leukocyte antigen (HLA) class II (Dominici et al., 2006). No single marker is able to identify an MSC, but collectively several positive markers are used to establish the presence of stromal cells. The negative markers are present on cells with a hematopoietic origin, e.g. immune cells. Lastly, the MSCs must be able to differentiate into osteoblasts, adipocytes, and chondrocytes (Bourin et al., 2013; Dominici et al., 2006). As the phenotypes of MSCs prepared from different adult tissues resemble

each other, the terms of ASC and MSC will be used interchangeably henceforth.

Especially ASCs seem promising for use in regenerative medicine as they are abundant and easy to procure. In addition, they are multipotent and can give rise to osteoblastic, chondrocytic, and adipocytic lineages (Bourin et al., 2013). ASCs can be isolated from human adipose tissue through enzymatic digestion, resulting in a stromal vascular fraction from which the stromal multipotent cells can be isolated (Gimble and Guilak, 2003; Bourin et al., 2013). When expanded and administered to a patient they will migrate to sites of injury where they secrete growth factors to promote a regenerative environment, and they are also potent regulators of both innate and the adaptive immune responses (Hidalgo-Garcia et al., 2018). Due to their regenerative and immunomodulatory properties the ASCs have been studied in relation to wound healing and various diseases such as graft versus host disease and cardiovascular diseases, where they show promising therapeutic effect (Bian et al., 2022; Luz-Crawford et al., 2017; Stevens et al., 2020).

In general, ASCs interact with their environment through either paracrine signalling or cell-cell contact. In an inflammatory environment, the ASCs can interact with immune cells to regulate their function, and many of the implicated modes of action of ASCs suggest that they act either directly or indirectly on macrophages (Luz-Crawford et al., 2017; Stevens et al., 2020). Therefore, it is difficult to identify a sole mechanism of action, and as a result also to anticipate experimental outcomes or demonstrate reproducible results, which in turn poses a challenge in designing a suitable potency assay (Bravery et al., 2013; Stevens et al., 2020).

## 6.1 Anti-Fibrotic Effects of Adipose-Stromal Cells

Cellular therapies based on ASCs have been used to promote regeneration of tissue and prevent fibrosis. Fibrosis can develop as a result of continued or chronic inflammation in the tissue, which causes excessive production of extracellular matrix (ECM) and scarring. Fibrosis can lead to decreased functionality of a tissue, and is characteristic in the progression of chronic diseases in different tissues such as the heart and kidneys (Guillamat-Prats, 2021; Kendall and Feghali-Bostwick, 2014; Setten et al., 2022). When tissue is injured the surrounding cells facilitate a response, which involves a series of overlapping events jointly called wound healing. These events are highly coordinated in order to attain optimal tissue regeneration, and start with the formation of a clot to prevent exsanguination with subsequent recruitment of immune cells (Figure 6.1A) (Guillamat-Prats, 2021). ASCs affect all phases of wound healing by promoting coagulation in the hemostatic phase, and modulating the inflammatory and proliferative phases by targeting immune responses to facilitate regeneration and repair of the tissue. Lastly, they secrete cytokines and growth factors that promote reorganization of collagens to remodel the tissue (Figure 6.1C) (Guillamat-Prats, 2021; Bian et al., 2022). ASCs can be activated by pro-inflammatory cytokines like interferon (IFN)- $\gamma$ . When activated, they have been shown to modulate immune cell response to tissue damage by decreasing production of pro-inflammatory cytokines while

promoting an anti-inflammatory environment. This happens through secretion of paracrine soluble factors such as transforming growth factor (TGF)- $\beta$ , interleukin (IL)-4, and IL-10, that can shift the balance in cytokine release between type 1 T helper (Th1) cells and type 2 T helper (Th2) cells. As such, ASCs can avert and/or reduce chronic inflammation and attenuate fibrosis (Guillamat-Prats, 2021; Bian et al., 2022).

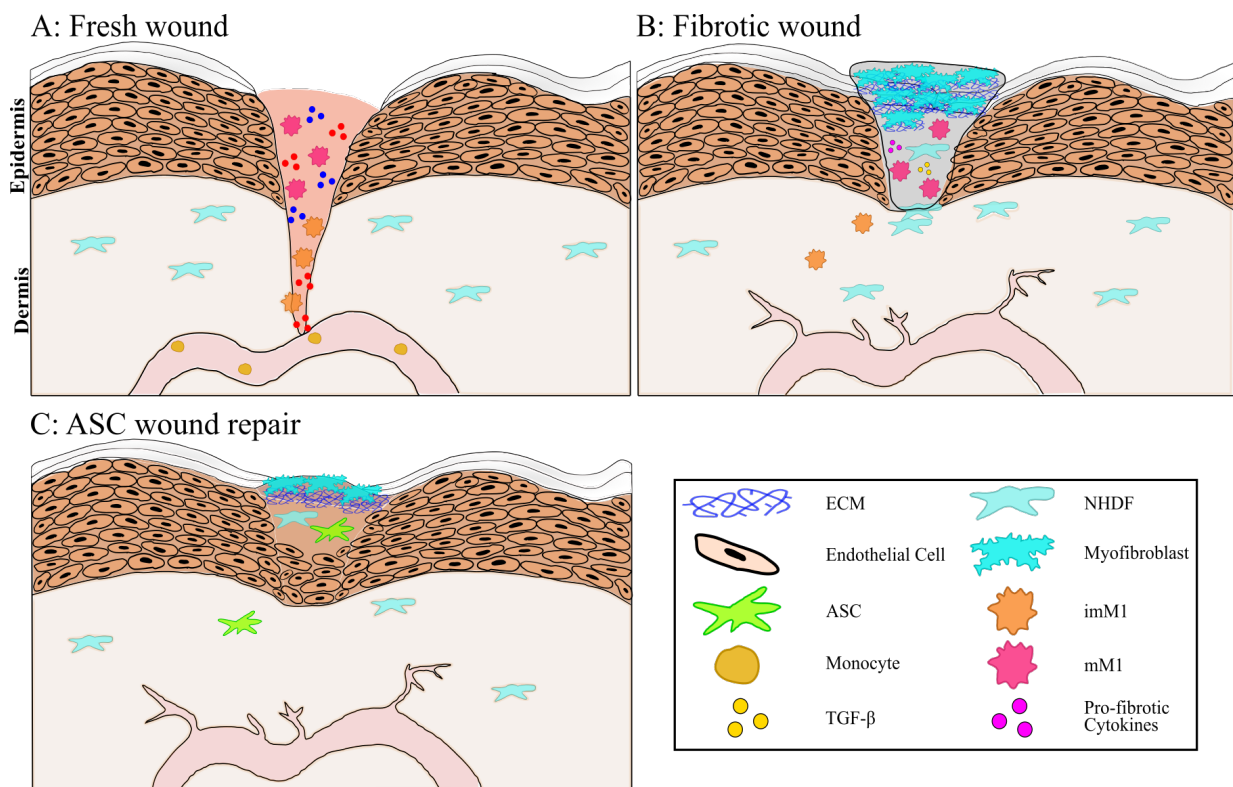


**Figure 6.1: ASCs in wound healing.** A: Firstly, a fibrin clot is formed in response to immediate tissue injury to prevent bleeding. Next, immune cells and fibroblasts migrate to the site of injury. The immune cells eliminate pathogens in the wound site, and the fibroblasts assist in recruitment of immune cells, and begin producing components of the ECM and differentiate into myofibroblasts. B: If the inflammatory phase is prolonged, activated fibroblasts will continue to recruit immune cells, thus creating a positive feedback loop. This further stimulates differentiation of fibroblasts into myofibroblasts which, if unregulated, will produce excessive amounts of ECM and result in increased deposition of ECM, leading to rigidity of the tissue and eventually loss of function. The grey area illustrates increased stiffness of the fibrotic tissue. C: Treatment with ASCs promotes coagulation and modulates the immune cell response by decreasing the production of pro-inflammatory cytokines by immune cells, thus promoting an anti-inflammatory milieu. They further increase migration of fibroblasts to promote proliferation of the ECM, and later secrete growth factors to aid in neovascularisation, reorganization and remodelling of the tissue along with repopulation of the injured area with endothelial cells. ASC: adipose-derived stromal cell, imM1: immature macrophage, mM1: mature macrophage, NHDF: normal human dermal fibroblast, ECM: extracellular matrix, TGF- $\beta$ : transforming growth factor- $\beta$ .

When tissue is injured, immune cells and fibroblasts respond by migrating to the site. They then start secretion of growth factors and proteins to repair the injury (Figure 6.1A). Scar formation happens when the injured tissue is replaced with pathological connective tissue (Kendall and Feghali-Bostwick, 2014; Guillamat-Prats, 2021). Connective tissue consists primarily of fibroblasts in an ECM, and fibroblasts are important in both maintenance and degradation of the ECM, as well as in wound healing, inflammation, angiogenesis, and in pathological tissue fibrosis (Kendall and Feghali-Bostwick, 2014).

The ECM is a network of proteins that provide tissue structure, and it is produced and maintained by fibroblasts. The ECM is composed of two subunits: The interstitial connective tissue matrix and the basement membrane. The interstitial matrix consists mainly of fibrillar proteins such as collagen I that provides tensile strength, and elastin, which allows for expansion of tissues (Zhao et al., 2022; Kendall and Feghali-Bostwick, 2014). The remodelling and reabsorption of the ECM is important in healing of tissue injury and in prevention of fibrosis. It is controlled through secretion of matrix metalloproteinase (MMP)s and tissue inhibitor of metalloproteinase (TIMP)s, which regulate the turnover rate of collagen (Guillamat-Prats, 2021). Excessive deposition of ECM is a common feature in fibrosis, and alterations in the constitution of the ECM can result in release of biologically active fragments. These are known as matricryptins, which were originally encapsulated within the ECM, and upon release they can affect both cell-cell and cell-ECM interactions (Zhao et al., 2022). The interstitial matrix also contains adhesive proteins such as fibronectin that connects the ECM to the surrounding cells by facilitating interactions with integrins through arginine-glycine-aspartic acid (RGD)-domains. The basement membrane is a hydrated gel made of proteoglycans, whose main function is to facilitate intercellular communications, and it is also a pathway for flow of nutrients into unvascularized tissues (Zhao et al., 2022; Kendall and Feghali-Bostwick, 2014).

Fibroblasts can be activated in response to cytokines such as TGF- $\beta$ . Activated fibroblasts secrete pro-inflammatory cytokines and contribute to the inflammatory milieu by promoting activation and migration of immune cells, which can result in chronic inflammation and fibrosis (Kendall and Feghali-Bostwick, 2014). They differentiate into myofibroblasts, which are important in tissue regeneration because they are highly contractile and have increased expression of cytokines, chemokines, and cell surface receptors. In addition, myofibroblasts are characterised by excessive production of ECM, which in turn promotes further recruitment of immune cells such as macrophages to the site of injury (Kendall and Feghali-Bostwick, 2014). In fibrosis, the differentiation of myofibroblasts is promoted through positive feedback regulation, which can result in increased amounts of collagen in the tissue, leading to increased rigidity and eventually loss of function (Figure 6.1B) (Zhao et al., 2022).

## 6.2 Macrophages

Macrophages are important immune modulators due to both their functional plasticity and their prevalence in the body (Stevens et al., 2020). They are large cells with varying morphology that depends on their activation state, and while macrophages have multiple functions in the body, their primary function is phagocytosis of pathogens and debris. Other than that, they are important antigen-presenting cells, they produce cytokines, and are able to both promote inflammation and aid in the repair of damaged tissue (Agger et al., 2015; Shapouri-Moghaddam et al., 2018). Some tissues such as the liver and lungs have resident macrophages, but macrophages can also be recruited as monocytes in the mononuclear phagocyte system (Agger et al., 2015). Monocytes migrate to sites of injury in response to pathogen-associated molecular pattern (PAMP)s and damage-associated molecular pattern (DAMP)s, and their phenotype can change in response to the elicited immune response and the environmental stimuli (Das et al., 2015; Shapouri-Moghaddam et al., 2018). A common denominator of the cells in the mononuclear phagocyte system is plasticity of their gene expression patterns, which means they are generally challenging to identify based on surface markers alone (Das et al., 2015).

The two major stimulating factors for differentiation of monocytes into macrophages are granulocyte macrophage colony stimulating factor (GM-CSF) and macrophage colony stimulating factor (M-CSF) (Jaguin et al., 2013). The proteins have different patterns of expression and induce different responses in monocytes and macrophages. M-CSF is produced ubiquitously and is expressed in a constitutive manner during homeostasis (Ushach and Zlotnik, 2016). GM-CSF is mainly produced by activated leukocytes as a part of the host response in the presence of an infectious agent. The monocyte-derived macrophages are immature until they receive an activating stimuli, and based on whether they are differentiated using GM-CSF or M-CSF, respectively, they are inclined to adopt a more pro-inflammatory or anti-inflammatory phenotype (Ushach and Zlotnik, 2016; Jaguin et al., 2013).

### Macrophage Phenotypes

Macrophages are matured in response to different activating stimuli. Mature macrophages are generally characterized by plasticity and flexibility, and can have either pro-inflammatory or anti-inflammatory properties, which is illustrated by distinct functional phenotypes (Das et al., 2015). There are two major macrophage phenotypes, which are classified based on whether they are polarised by cytokines secreted by Th1 or Th2 cells (Das et al., 2015). Th1-cytokines such as IFN- $\gamma$  or tumor necrosis factor (TNF)- $\alpha$  produce classically activated macrophages, known as mature M1 (mM1) macrophages that support Th1-mediated immune responses and are pro-inflammatory. On the other hand, Th2-cytokines like IL-4 and IL-10 induce a non-classically activated macrophage phenotype, which is anti-inflammatory and support Th2-functions (Das et al., 2015). These will be referred to as mature M2 (mM2) macrophages.

When macrophages are activated, they increase their expression of antigen-presenting and co-stimulatory molecules such as CD80 and CD86, and HLA-DR (Shapouri-Moghaddam et al., 2018). The mM1 and mM2 macrophage phenotypes have different expression profiles and produce different cytokines to support their roles in attenuation and resolution of inflammation, respectively (Appendix A.1).

These differences can be used to determine their polarisation state (Shapouri-Moghaddam et al., 2018; Luz-Crawford et al., 2017). The polarisation state of a mature macrophage depends on the presence of stimuli in the local tissue environment, which can promote both recruitment and differentiation of monocytes into macrophages, and maturation or repolarisation of existing macrophages. While the distinct macrophage phenotypes can be induced *in vitro*, it is more likely that the macrophage population *in vivo* is constantly changing due to a multitude of stimuli (Hidalgo-Garcia et al., 2018).

The mM1 macrophages are activated as an immediate response to e.g. tissue injury through inflammatory signals like IFN- $\gamma$ , or by the presence of pathogens or bacterial toxins such as lipopolysaccharide (LPS). They typically have a high expression of pro-inflammatory cytokines, for example TNF- $\alpha$  and IL-12. Additionally, the mM1 macrophages have a high expression of Th1-attracting chemokines like C-X-C motif chemokine ligand (CXCL)9 and CXCL10, which increase recruitment of T cells (Shapouri-Moghaddam et al., 2018). The production of these cytokines ensues antigen presentation, promotion of Th1 responses, and production of reactive oxygen species, all of which promote the cytotoxic adaptive immunity and lead to upregulation of co-stimulatory molecules (Luz-Crawford et al., 2017; Shapouri-Moghaddam et al., 2018).

Different mM2 macrophage subgroups exist: The M2a, M2b, and M2c subsets, each with different characteristics (Shapouri-Moghaddam et al., 2018). The best known is the M2a subset, which can be stimulated by IL-4 and IL-13, has an anti-inflammatory phenotype, and is involved in tissue remodelling. The M2b subset is induced by exposure to immune complexes and through toll-like receptors, while the M2c subset has an immunosuppressive phenotype that promotes neovascularization and can be induced by stimulation with IL-10, TGF- $\beta$ , or glucocorticoids (Das et al., 2015). The mM2 macrophages are present in the later stages of macrophage recruitment e.g. after tissue injury. They produce anti-inflammatory cytokines such as TGF- $\beta$  and IL-10, have a high expression of scavenger receptors and C-type lectin receptors like CD206, and they also secrete chemokines to recruit Th2 cells, regulatory T cells and neutrophils (Luz-Crawford et al., 2017; Shapouri-Moghaddam et al., 2018). The mM2 macrophages tend to have a higher phagocytic activity than the mM1 macrophages, as phagocytosis of dead or apoptotic cells and debris inhibits the production of pro-inflammatory cytokines and also involves secretion of TGF- $\beta$ , which inhibits recruitment of monocytes and macrophages. Furthermore, phagocytosis limits local inflammation by protecting the tissue from both pro-inflammatory cytokines and immunogenic components of the debris (Shapouri-Moghaddam et al., 2018).

When tissue is injured, macrophages are recruited to the site, and are hereafter matured into mM1 macrophages in response to DAMPs and PAMPs. They begin to secrete pro-inflammatory cytokines and further contribute to the activation and proliferation of fibroblasts. Later, macrophages can be repolarised into mM2 macrophages that help degrade ECM components and inhibit the activity of fibroblasts and myofibroblasts, thereby aiding in resolution of inflammation (Kendall and Feghali-Bostwick, 2014; Zhao et al., 2022). The ECM is continuously produced and degraded in an equilibrium to maintain tissue homeostasis. Macrophages produce MMPs to degrade the ECM, and can also ingest ECM components to resolve inflammation and promote a regenerative environment. This is key in restoring ECM homeostasis after tissue injury to prevent continuous deposition of ECM (Figure 6.2). If the macrophage-MMP-ECM balance is disrupted, it can result in excessive deposition of ECM, thereby creating a positive feedback loop that leads to fibrosis (Zhao et al., 2022; Kendall and Feghali-Bostwick, 2014).

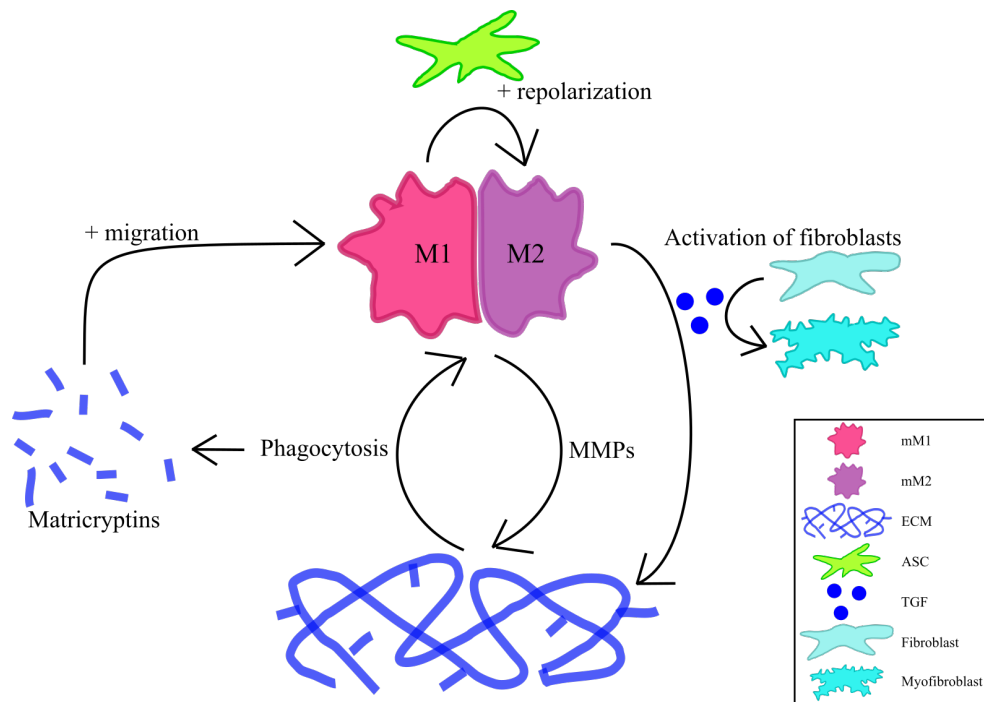


**Figure 6.2: Interactions between macrophages and the ECM.** Macrophages can regulate the degradation of ECM by producing MMPs and through ingestion of ECM, resulting in release of matricryptins. This can further promote migration of monocytes and activation of mM1 macrophages. ASCs can induce repolarisation of macrophages towards an mM2 phenotype that secretes TGF- $\beta$ , causing fibroblasts to differentiate into myofibroblasts. This further promotes remodelling of the ECM during normal tissue repair. Disrupting the macrophage-MMP-ECM balance can lead to the promotion of differentiation of myofibroblasts through a positive feedback loop that results in an increased deposition of ECM, eventually leading to fibrosis. MMP: Matrix metalloproteinase, mM1: mature M1 macrophage, mM2: mature M2 macrophage, ECM: Extracellular matrix, ASC: Adipose-derived stromal cell, TGF: Transforming growth factor- $\beta$ .

ASCs have been shown to induce M2-like polarisation of monocytes and monocyte-derived macrophages in *in vitro* models and also to prevent LPS- or IFN- $\gamma$ -induced mM1 polarisation, thus modulating macrophage function (de Witte et al., 2018; Hidalgo-Garcia et al., 2018). This suggests that macrophages play a critical part in the therapeutic effect of ASCs, because the ASC-induced migration and repolarisation of mM2 macrophages to a site of injury promotes tissue regeneration (Luz-Crawford et al., 2017).

## Potential Regenerative Properties of Macrophages

The function of macrophages is crucial in both the innate and the adaptive immune system, as they acquire information from their surroundings and communicate it by presenting antigens, thus facilitating a coordinated immune response (Jaguin et al., 2013). Just as macrophages and other immune cells are recruited and home to sites of injury, ASCs have demonstrated this ability when administered as a therapy. However, when administered through intravenous infusion, the ASCs end up being trapped in the lungs with no evidence of engraftment, meaning the life-span of ASCs *in vivo* is relatively short (Bian et al., 2022; Stevens et al., 2020). The ASCs exert their paracrine effects by the release of extracellular vesicles, and through their secretome they can induce a phenotypic switch in macrophages from an mM1 to an mM2 phenotype (Bian et al., 2022). While the paracrine effects of ASCs seem to play an important role in their mode of action, the complex communication between macrophages and ASCs also includes direct cell-cell contact. Macrophages phagocytise apoptotic cells, which can result in immunosuppression and so, uptake of ASCs or ASC-derived cytoplasmic components by macrophages can also result in repolarisation of macrophages from an mM1 phenotype to a functional mM2 phenotype. In fact even apoptotic, fragmented or inactivated ASCs may be able to exert their immunomodulatory functions on macrophages due to the clearance of apoptotic ASCs by phagocytising macrophages (de Witte et al., 2018; Shapouri-Moghaddam et al., 2018; Stevens et al., 2020). mM1 macrophages in coculture with ASCs have a higher upregulation of genes involved in immunosuppression when compared to mM2 macrophages cocultured with ASCs. This further suggests that the crosstalk between macrophages and ASCs is vital for the regenerative effects of ASCs (Stevens et al., 2020). The mM2 macrophage phenotype may be able to assist in survival, proliferation and migration of ASCs, thereby creating a positive feedback loop, where LPS-induced release of TNF- $\alpha$  by the macrophages can stimulate the ASCs, causing them to secrete growth factors to promote tissue repair (Luz-Crawford et al., 2017).

## 6.3 Aim of Study

The aim of this study was to develop a macrophage-ASC-coculture model to investigate whether treatment of macrophages with ASCs could polarise the macrophages towards a phenotype that could attenuate fibrosis in a fibroblast-derived ECM-model.

To achieve this aim, two main objectives were addressed:

- To investigate the effect of different concentrations of LPS and IFN- $\gamma$  on a macrophage and ASC coculture.
- To investigate the effect of ASC-treated macrophages on the ECM model.

The hypotheses were:

- Optimal experimental concentrations of LPS and IFN- $\gamma$  will allow for detection of the effect of the ASCs on macrophage activation, e.g. in terms of TNF- $\alpha$  secretion.
- Treatment of ECM with ASC-treated macrophages will result in decreased deposition of ECM when compared to ECM treated with mM1 macrophages, immature macrophages, or ECM without macrophages, e.g. regarding the levels of collagen type I and III.

## 7 | Methods

The experimental setup was comprised of multiple steps (Figure 7.1), and the final design of the study was based on additional supporting experiments. The final design is illustrated in figure 7.1, from isolation of monocytes to evaluation of the assays. The aim was to further optimise an existing model for differentiation of mM1 macrophages from cryopreserved peripheral blood mononuclear cell (PBMC)-derived monocytes, which were developed by Hansen et al. (2022). A number of experiments were conducted to achieve this aim, such as determining the optimal concentration of activating stimuli using enzyme-linked immunosorbent assay (ELISA), and with correction for cell count based on immunocytochemistry (ICC), and investigating PKH26-labelling of ASCs for evaluating macrophage phagocytosis. Different methods for separation of the macrophage and ASC (M1:ASC) coculture were tested, with the aim of using the isolated ASC-treated M1 (ASC-M1) macrophages in combination with an ECM-fibroblast-model. The ECM model was based on an existing Scar-in-a-Jar-model developed by Søndergaard et al. (2022).

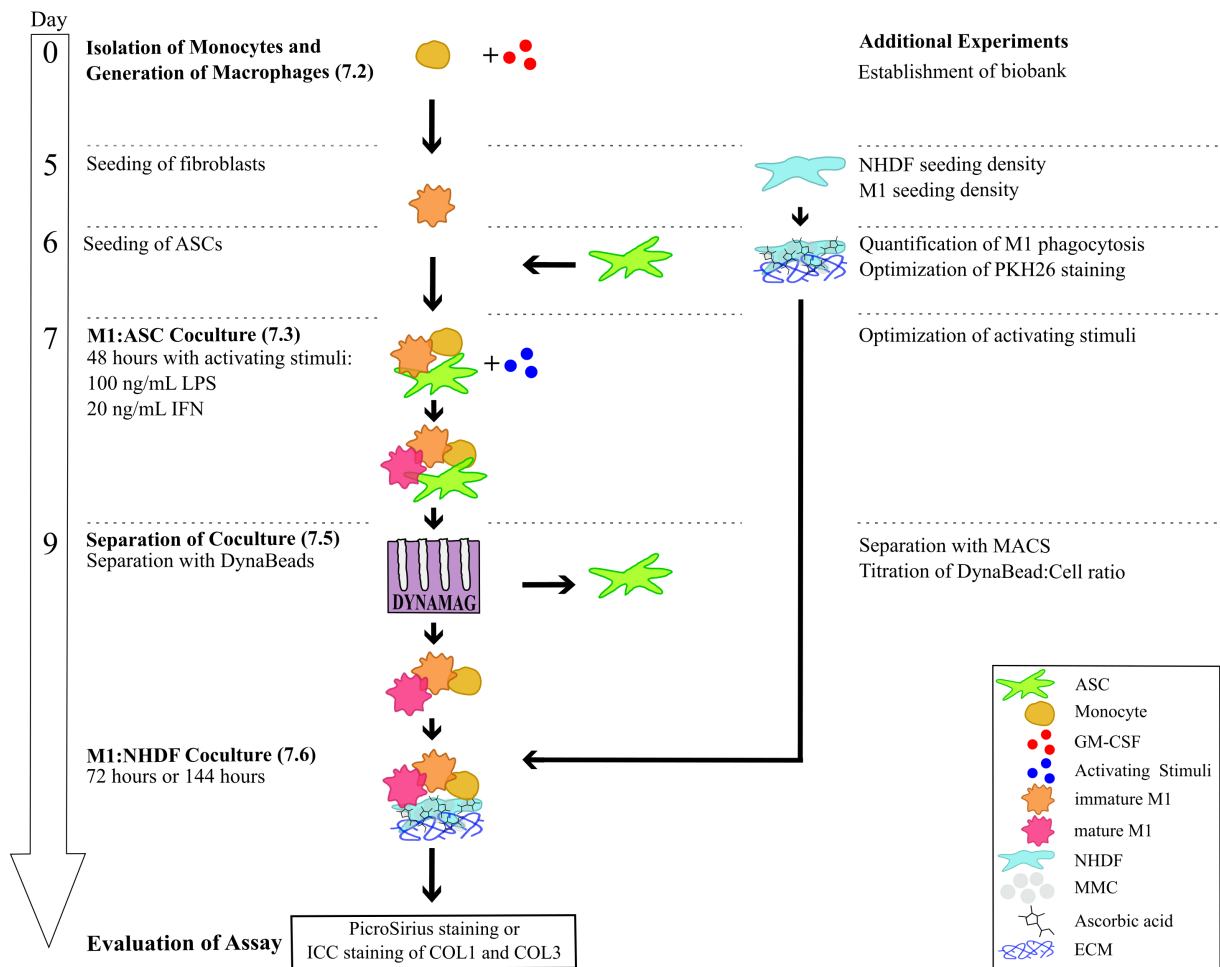


**Figure 7.1: Overview of the final experimental setup.** The experimental setup including any additional experiments that were performed. Left, the final setup is described with numbers indicating the respective sections where further details can be found. Middle, graphic depiction of the study design. Right, the additional experiments are listed. LPS: lipopolysaccharide, IFN: interferon- $\gamma$ , TNF: tumor necrosis factor- $\alpha$ , ELISA: enzyme linked immunosorbent assay, ICC: immunocytochemistry, MACS: magnetic-activated cell sorting, FACS: fluorescence-activated cell sorting, ASC: adipose-derived stromal cell, GM-CSF: granulocyte-macrophage colony stimulating factor, M1: M1 macrophage, NHDF: normal human dermal fibroblast, MMC: macromolecular crowders, AA: ascorbic acid, ECM: extracellular matrix

## 7.1 Cryopreservation of Peripheral Blood Mononuclear Cells

Buffy coats were obtained from the Bloodbank at Rigshospitalet in order to establish a biobank of cryopreserved PBMCs. This protocol had previously been optimised by Hansen et al. (2022). Buffy coats were diluted 1:3.6 in 1x PBS (Gibco, cat. no. 10010-015) supplemented with fetal bovine serum (FBS) (2%,  $\gamma$ -irradiated, heat-inactivated) (Gibco, cat. no. 10101-145) (FBS-PBS). This is appropriate for transfer to six LeucoSep tubes (Greiner Bio-one, cat. no. 227290) with Lymphoprep (Alere Technologies, cat. no. 04-03-9391/02). The diluted buffy coats were centrifuged at 800g for 15 minutes at room temperature (RT) (acceleration (A)=9; deceleration (D)=1), then the plasma phase was removed. The interphases were poured into a new centrifuge tube, divided into four new centrifuge tubes and filled with FBS-PBS, before centrifugation at 300g for five minutes (RT, A=9; D=5). Unless otherwise stated these are the settings for centrifugation. The four tubes were pooled into two tubes, and the process was repeated. To collect as many cells as possible, the emptied tubes were washed with FBS-PBS. The cell suspension was strained through a cell strainer (40  $\mu$ m) (Fisher Scientific, cat. no. 22-363-547) into a single tube, and counted on a NC-202 (Nucleocounter) (Chemometec, NC-View 2.2.0.21) in a 1:20 dilution with PBS using a protocol suited for PBMCs. The cell concentration was adjusted to 2E7 cells/mL in cryomedium consisting of FBS with dimethyl sulfoxide (DMSO) (10%) (WAK-Chemie, cat. no. USP20131), and transferred to cryovials (1 mL/vial). Cryovials were then placed in a cold CoolCell container and cooled at 4 °C for 10 minutes before storage at -80 °C overnight. The next day, the cryovials were transferred to liquid nitrogen for long-term storage.

## 7.2 Isolation of Monocytes and Generation of Macrophages

The experimental setup started on day zero (Figure 7.1), with isolation of monocytes from cryopreserved PBMCs by magnetic-activated cell sorting (MACS) using an LS column (Miltenyi Biotec, cat. no. 130-042-401) and MACS buffer consisting of 1x PBS with ethylenediaminetetraacetic acid (EDTA) (2 mM) (Invitrogen, AM9260G) and FBS (0.5%,  $\gamma$ -irradiated, heat-inactivated). The protocol for isolation of monocytes and generation of macrophages was also previously optimised by Hansen et al. (2022). Before thawing of PBMCs, the MACS buffer was degassed in vacuum for 10 minutes using a Steriflip filter system (0.22  $\mu$ L membrane) (Milipore, cat. no. SCGP00525). Both the MACS buffer and the LS column were kept at 4 °C to prevent trapping of cells.

Cryopreserved PBMCs were thawed in a water bath (37 °C), transferred to a centrifuge tube filled with PBS to 10 mL, and centrifuged before the supernatant was removed completely. The cells were adjusted to 1E8 cells/mL in MACS buffer, and incubated with 40  $\mu$ L of CD14 MicroBeads (Miltenyi Biotec, cat. no. 130-050-201) per 8E7 PBMCs for 15 minutes at 4 °C, and then washed in MACS buffer. Unless otherwise stated, washing steps were

followed by centrifugation and discarding of supernatant. Meanwhile, an LS column was placed on a MidiMACS<sup>TM</sup> separator (Miltenyi Biotec, cat. no. 130-042-302) and washed by letting 3 mL of MACS buffer drain through. The PBMCs were carefully resuspended in 3 mL of MACS buffer, transferred to the LS column, and washed three times by letting MACS buffer drain through to ensure that unbound cells were removed. The column was removed from the separator, the cell solution was gently forced into a new centrifuge tube using 5 mL of MACS buffer, and counted on a NC-202. The cell concentration was adjusted to 5E5 cells/mL, resulting in 65,789 cells/cm<sup>2</sup> in complete medium consisting of RPMI-1640 (Sigma-Aldrich, cat. no. R8758) supplemented with FBS (10%,  $\gamma$ -irradiated, heat-inactivated) and Penicillin-Streptomycin (Pen/Strep) (100 U/mL) (Gibco, cat. no. 15140-122), and 0.5 mL/well was seeded in an untreated 12-well plate (Thermo Scientific, cat. no. 150200). To differentiate the isolated monocytes into macrophages, 0.5 mL of 2x polarising medium consisting of recombinant human GM-CSF (20 ng/mL) (Peprotech, cat. no. 300-03) in complete medium was added to each well, before incubation at 37 °C and 5% CO<sub>2</sub> for two-three days. These are the conditions used for incubation of cells.

On day two or three (Figure 7.1), 1 mL of fresh 2x polarising medium was added to each well, before incubation for another two-three days. On day five or six, 1 mL of medium was carefully removed from each well, and replaced with 1 mL of fresh 2x polarising medium, before incubation until harvest and coculture with ASCs on day seven.

### 7.3 Coculture of Macrophages and ASCs

Cryopreserved ASCs (CSCC, Donor ID ASC\_BO03) had previously been isolated by enzymatic digestion of lipoaspirate from a consenting, healthy volunteer (Søndergaard et al., 2022) in compliance with the Declaration of Helsinki (World Medical Association, 2001). On day six (Figure 7.1), the ASCs were thawed in a water bath (37 °C), transferred to a centrifuge tube filled to 10 mL with complete medium and centrifuged. The cells were adjusted to 5,000 cells/cm<sup>2</sup> (4.8E4 cells/mL), seeded into an untreated 6-well plate (1 mL/well) (VWR, cat. no. 734-2777), and incubated overnight.

On day seven (Figure 7.1), the monocyte-derived macrophages were harvested by centrifuging the plates, washing in 1 mL of PBS, centrifuging again, and then incubating in 1 mL of TrypLE (Gibco, cat. no. 12563-029) for 20 minutes at 37 °C. The cells were released by pipetting and transferred to a centrifuge tube. Cell release was validated using a microscope. The wells were washed once with 1 mL of PBS, and the TrypLE was inactivated by adding equal volume of complete medium. The cell concentration was adjusted to 25,000 cells/cm<sup>2</sup> (2.4E5 cells/mL), before 1 mL of macrophage cell suspension was seeded in each well containing ASCs.

The M1:ASC coculture was activated by adding 1 mL of 4x LPS (400 ng/mL) (Sigma-Aldrich, cat. no. L3024) in 2x polarising medium and 1 mL of 4x IFN- $\gamma$  (80 ng/mL) (Peprotech, cat. no. 300-02) in 2x polarising medium to each well. The coculture was

then incubated for 48 hours. Optimal concentrations of activating stimuli was determined by ELISA and is described below. For setups that included immature macrophages as controls, no activating stimuli was added to the polarising medium.

## 7.4 Validation of the Macrophage Model

### Determination of Optimal Activating Stimuli

The optimal concentrations of activating stimuli were determined through titration of LPS and IFN- $\gamma$ . The M1:ASC coculture was seeded in a black 96-well plate with a clear bottom (Costar, ref. 3603) and activated with different concentrations of stimuli in all combinations through a five-fold serial dilution from 500 ng/mL to 20 ng/mL (LPS) or 100 ng/mL to 5 ng/mL (IFN- $\gamma$ ), respectively (Table 7.1). The coculture was incubated with activating stimuli for 48 hours before supernatants were harvested for ELISA analysis.

500 ng/mL LPS 100 ng/mL IFN- $\gamma$	100 ng/mL LPS 100 ng/mL IFN- $\gamma$	20 ng/mL LPS 100 ng/mL IFN- $\gamma$
500 ng/mL LPS 20 ng/mL IFN- $\gamma$	100 ng/mL LPS 20 ng/mL IFN- $\gamma$	20 ng/mL LPS 20 ng/mL IFN- $\gamma$
500 ng/mL LPS 5 ng/mL IFN- $\gamma$	100 ng/mL LPS 5 ng/mL IFN- $\gamma$	20 ng/mL LPS 5 ng/mL IFN- $\gamma$

**Table 7.1: Titration of activating stimuli.** Concentrations of LPS and IFN- $\gamma$  for the titration of optimal activating stimuli. LPS: Lipopolysaccharide, IFN- $\gamma$ : IFN- $\gamma$

The ELISA was performed using an ELISA kit for determination of TNF- $\alpha$  concentrations (Human TNF- $\alpha$  DuoSet ELISA, DY210-05 and DuoSet ELISA Ancillary Reagent Kit 2, DY008) over the course of three days. The ELISA test was performed twice to determine the proper dilution of the supernatant, and to test the levels of TNF- $\alpha$  in the samples. The samples were serial diluted five-fold in Reagent Diluent from 1x to 125x.

On day one, the plate was coated with Capture Antibody (4  $\mu$ g/mL). On day two, the plate was washed three times in an ELISA platewasher (Tecan Hydrospeed Platewasher, cat. no. 1919995985) using a predefined program to wash the plate three times by removing supernatant and adding 200  $\mu$ L of washing buffer (Program QC 3x200  $\mu$ L). This was used for all washing steps. The plate was blocked with Reagent Diluent and incubated at RT for one hour. In the meantime, the samples were diluted, and the standard solutions of TNF- $\alpha$  were prepared by two-fold serial dilution from 1,000 pg/mL to 15.6 pg/mL. After incubation, the plate was washed and incubated with standard solutions and diluted samples at 4  $^{\circ}$ C overnight. On day three, the plate was washed and incubated for two hours with detection antibody. Streptavidin-Horse Radish Peroxidase was added for 20 minutes at RT in the dark, then substrate solution was added for 20 minutes at RT, also in the dark. At last, stop solution was added and the plate was measured at 450 nm on

a FLUOstar Omega ELISA reader (Omega v5.5.0.R.3). To correct for optical impurities the background was measured at 540 nm and subtracted. Furthermore, the samples were corrected based on a blank sample. Omega Mars software (BMG Labtech, v3.32 R4) was used to plot the standard curve, and a 5-parameter fit was chosen for determination of TNF- $\alpha$  concentration based on the range of standards. The 5-parameter fit was chosen over a 4-parameter fit or a linear fit due to a higher coefficient of determination. Data from the ELISA can be seen in Appendix A.2 and A.3.

The cocultures were fixated in 4% paraformaldehyde in PBS (Hospital Pharmacy, cat. no. 861215) for 20 minutes at RT, and the concentration of TNF- $\alpha$  was normalised to cell count with ICC. The following stains and antibodies were used to stain the cocultures: Hoechst 33342 (2  $\mu\text{g}/\text{mL}$ ) (Invitrogen, cat. no. H3570), primary antibody: Mouse anti-Human CD45 Antibody Cocktail (2  $\mu\text{g}/\text{mL}$ ) (Invitrogen, cat. no. MA5-12197) and secondary antibody: Rabbit anti-Mouse IgG (H+L) Cross-Adsorbed Secondary Antibody, AF555 (5  $\mu\text{g}/\text{mL}$ ) (Invitrogen, cat. no. 10728994) diluted in PBS. To do the staining, the PBS was removed from the wells, before they were blocked in 1% bovine serum albumine (BSA) (Tocris, cat. no.5217) for 30 minutes at RT, incubated with Hoechst stain for 15 minutes at RT, and then washed in PBS. Fluorescent images were acquired at this step for safety in case the cells were washed away during antibody staining. The cells were incubated with the primary antibody at 4  $^{\circ}\text{C}$  overnight, and washed in PBS the following day, before adding the secondary antibody for one hour at RT in the dark. The wells were carefully washed twice in PBS prior to analysis on a fluorescent microscope.

## Titration of Optimal Concentration of PKH26

Labelling of the ASC-membrane using PKH26 dye was introduced as a method for evaluating whether the macrophages phagocytised the ASCs during coculture. The titration of optimal concentration of PKH26 membrane stain was performed twice using a PKH26 Red Fluorescent Cell Linker Mini Kit (Sigma-Aldrich, cat. no. MINI26-1KT), and cryopreserved ASCs, which were thawed, centrifuged and washed in 1 mL of serum-free RPMI-1640 medium. The ASC concentration was adjusted to 2E6 cells/mL in Diluent C using a NC-202. Standard solutions of the PKH26 dye were prepared by a two-fold serial dilution, first from 40  $\mu\text{M}$  to 2.5  $\mu\text{M}$  and second, from 20  $\mu\text{M}$  to 0.625  $\mu\text{M}$ , and both times a Diluent C vehicle control and an unstained control were included. ASCs were added to each standard dye solution (1E5 cells/tube) and incubated for four minutes at RT, during which the tubes were gently flicked every minute, until the staining was stopped by adding equal volume of FBS followed by centrifugation. Cell pellets were washed three times, and after the last washing step, the cells were counted on a NC-202, centrifuged, and resuspended in 1 mL of complete medium. Hereafter, they were seeded in a 6-well plate and incubated for three days.

On day three, the ASCs were harvested to FACS tubes (Falcon, cat. no. 352054), centrifuged, resuspended in FVS450 dye (0.125  $\mu\text{g}/\text{mL}$  in PBS) (BD Biosciences, cat. no. 562247), and incubated for 15 minutes at RT in the dark. The tubes were washed once in

2 mL of FACS buffer, consisting of FBS (10%), EDTA (1 mM) (Hospital Pharmacy, cat. no. 850097), and sodium azide (0.05%, v/w) in PBS, then centrifuged, and resuspended in 200  $\mu$ L of FACS buffer before analysis on a flow cytometer (for additional details, see section 7.8).

## 7.5 Separation of the Coculture

Separation of the M1:ASC coculture was done on day nine (Figure 7.1). Initially, it was tested whether harvest with TrypLE was sufficient to create a single cell suspension on a NC-202 which, besides cell numbers and viability, provides an image along with an estimate of the percentage of aggregation.

At first, separation of the coculture was tested with MACS. The harvested cell suspension was centrifuged and adjusted to 1E8 cells/mL in cold MACS buffer, labelled with 20  $\mu$ L of CD90 Microbeads (Miltenyi Biotec, cat. no. 130-096-253) per 1E7 cells, and incubated for 15 minutes at 4 °C. MACS buffer was added for a final volume of 5 mL, and the cells were centrifuged and resuspended in 3 mL of MACS buffer. An LS column was washed before the cell solution was pipetted into the column, as previously described. Both the negatively selected cells and the positively selected cells were counted on a NC-202 to assess the separation.

DynaBeads were used for separation of the M1:ASC coculture. The optimal number of Dynabeads per cell was determined by titration with 20 beads/cell, 10 beads/cell, and 5 beads/cell. Before harvesting the coculture, 25  $\mu$ L of Dynabead Pan Mouse IgG (1E7 beads) (Invitrogen, cat. no. 110.41) per 5E5 cells/mL were washed in 1 mL of MACS buffer, and placed in a DynaMag<sup>TM</sup>-5 Magnet (Invitrogen, cat. no. 12303D) for one minute before the supernatant was discarded and the washed beads were resuspended in MACS buffer to initial volume. The beads were coated with CD90 Mouse anti-Human Monoclonal Antibody F15-42-1 (1:1000) (1  $\mu$ g/mL) (Invitrogen, cat. no. MA1-81930) for 30 minutes at 4 °C in the dark with gentle tilting and rotation to prevent settling of beads. The coated beads were washed twice in MACS buffer while placed in the magnet, before removal from the magnet and resuspension to initial volume. The M1:ASC coculture was harvested, and an unseparated sample was extracted for analysis on the flow cytometer. The coculture was incubated with the CD90-coated beads (20 beads/cell) for 30 minutes at 4 °C in the dark with gentle tilting and rotation. An additional 1 mL of MACS buffer was added to limit cell trapping, and cells were sorted in a DynaMagnet for two minutes. While in the magnet, the supernatant with unlabelled cells were transferred to new tubes and counted on a NC-202, before the separation was evaluated on a flow cytometer by extracting samples from the sorted supernatants and comparing them to ASC and mM1 controls.

## 7.6 Evaluating the effect of ASC-treated Macrophages on the Extracellular Matrix

To create a scar-like ECM, cryopreserved normal human dermal fibroblasts (NHDF)s (Promocell, Passage 6) were cultured in Dulbecco's modified eagle medium (DMEM) medium consisting of DMEM (Thermo Fischer, cat. no. 31966-021) supplemented with FBS (0.4%,  $\gamma$ -irradiated) and Pen/Strep (100 U/mL). A titration was performed to determine the optimal concentration of fibroblasts through a two-fold serial dilution from 20E3 cells/cm<sup>2</sup> to 5E3 cells/cm<sup>2</sup>. Additionally, it was established whether the fibroblasts were able to produce sufficient amounts of ECM if TGF- $\beta$  was removed after three days.

On day five (Figure 7.1), fibroblasts were thawed in a water bath (37 °C), transferred to a centrifuge tube filled to 10 mL with DMEM medium, and centrifuged. The cell pellet was resuspended in 1 mL of DMEM medium, counted on a NC-202, adjusted to 10E3 cells/cm<sup>2</sup> (3.2E4 cells/mL), seeded in a black 96-well plate with a clear bottom (100  $\mu$ L per well) (Greiner Bio-One, cat. no. 9302), and incubated overnight. The next day, experimental conditions were created by adding 100  $\mu$ L of Ficoll medium to all wells. This consisted of ascorbic acid (0.033 mg/mL) (Wako, cat. no. 013-196441) and macromolecular crowding (MMC) generated with a ficoll solution that contained Ficoll 70 (37.5 mg/mL) (Cytiva, cat. no. 17031010) and Ficoll 400 (25 mg/mL) (Sigma Aldrich, cat. no. F4375). The concentrations of ficoll were based on findings by Chen et al. (2009). The Ficoll medium was supplemented with 2x Recombinant Human TGF- $\beta$  (10 ng/mL) (Peprotech, cat. no. 100-21), and the fibroblasts were incubated for 72 hours before the medium was changed by removing 160  $\mu$ L of Ficoll medium, washing in 160  $\mu$ L of PBS, and adding 160  $\mu$ L of fresh Ficoll medium, this time with no TGF- $\beta$ . Unless otherwise stated, this was how medium was changed in the ECM model, to prevent the ECM from drying out and to prevent any excess TGF- $\beta$  from affecting the macrophages. Other than an experimental control where TGF- $\beta$  was removed after three days when medium was changed, both positive and negative controls were included.

To determine the optimal seeding density of the fibroblasts, they were fixated in 4% paraformaldehyde in PBS after six days of experimental conditions. This was followed by washing for five minutes in 200  $\mu$ L of hydrochloric acid (HCL) (0.01 M) (Merck, cat. no. 1.09057) in PBS, and incubation with Sirius Red (0.1%) in Picric Acid (PicroSirius) (Hospital Pharmacy, cat. no. 856382) at RT overnight. The next day, the fibroblasts were washed for five minutes in HCL (0.01 M), and then twice in ion-exchanged water before analysis on a fluorescence microscope (see section 7.7 for further details). Wells were also stained with Hoechst, but this staining was incompatible with the PicroSirius dye.

To determine optimal seeding density of the macrophages, they were added to the fibroblasts after three days of experimental conditions. The optimal concentration of macrophages were determined through a two-fold serial dilution from 16E5 cells/mL to 0.1E5 cells/mL. On day nine (Figure 7.1), the macrophage and fibroblast (M1:NHDF) coculture was created

similarly to how the medium was changed, but instead 100  $\mu\text{L}$  of macrophage suspension and 100  $\mu\text{L}$  of fresh 2x Ficoll medium was added. Macrophages were isolated from the M1:ASC coculture using Dynabeads before they were centrifuged, resuspended in 1 mL of Ficoll medium, counted on a NC-202, and adjusted to 6,125 cells/ $\text{cm}^2$  (2E4 cells/mL). Macrophages from two donors were included in each setup, and mM1 macrophages were included for comparison with ASC-M1 macrophages after M1:NHDF coculture. Additionally, immature M1 (imM1) macrophage controls were included to determine whether the activation of macrophages improved their effect. Initially, the M1:NHDF coculture was fixated in 4% paraformaldehyde in PBS after three days of coculture with fibroblasts. However, to allow for more collagen deposition the study setup was extended. In the extended setup, the media was changed after three days of M1:NHDF coculture, followed by incubation for another three days, before fixation prior to immunocytochemical staining.

The immunocytochemical staining was performed using the following primary antibodies: Collagen I Mouse anti-Human Monoclonal Antibody (1:2000) (3.15  $\mu\text{g}/\text{mL}$ ) (Invitrogen, cat. no. MA1-26771) and Collagen III Rabbit anti-Human Polyclonal Antibody (1:300) (3.33  $\mu\text{g}/\text{mL}$ ) (Invitrogen, cat. no. PA5-99160) and secondary antibodies: Goat anti-mouse IgG AF488-conjugated (1:2000) (1  $\mu\text{g}/\text{mL}$ ) (Invitrogen, cat. no. A-11001) and Goat anti-rabbit IgG (H+L) AF546-conjugated (1:500) (4  $\mu\text{g}/\text{mL}$ ) (Invitrogen, cat. no. A-11035) diluted in 1%-BSA-PBS. Before adding the primary antibodies, the cells were permeabilised with Triton X-100 (0.3%) (Sigma-Aldrich, cat. no. X-100), washed twice in PBS, incubated for 15 minutes at RT, and then blocked in 1%-BSA-PBS for 30 minutes at RT. The cells were incubated in 100  $\mu\text{L}$  of primary antibody mastermix for one hour at RT, washed once in PBS, and then incubated in 100  $\mu\text{L}$  of secondary antibody mastermix for one hour at RT in the dark. Lastly, the cells were stained with Hoechst for 15 minutes at RT, before being washed twice in PBS, and analysed on a fluorescent microscope.

## 7.7 Microscopy

In order to document cell differentiation and their general well-being throughout the setup, images were obtained at each stage with an EVOS XL Core microscope using 10x, 20x, and 40x Olympus objectives (PH2 4x/10x or 20x/40x with condenser annulus). These images were also used in troubleshooting.

Fluorescent images were acquired using an inverted microscope (Axio Observer 7, Zeiss) fitted with scanning stage, microLED illumination for transmitted light, a HXP 120 V fluorescence light source, and an Axiocam 506 mono camera with Plan-Apochromat 5x, 20x and 40x objectives. Exposure time was fixed between samples, and separate channels were acquired based on the respective setups; this depended on the fluorescent tags of the secondary antibodies and the use of PicroSirius or Hoechst staining (Appendix A.4).

For the normalisation of TNF- $\alpha$  to cell count stitched images covering each well were acquired with a 5x objective, and then analysed in Fiji (ImageJ, v1.53t) using a macro

for automatic background subtraction, Gaussian Blur, Li Dark threshold (CD45) or Otsu threshold (Hoechst), watershedding, and particle analysis. Based on this, the concentration of TNF- $\alpha$  was normalised to picogram per thousand cells (pg/1,000 cells).

To determine optimal seeding densities of fibroblasts and macrophages, stitched images covering each well were acquired using the 5x objective along with five close-up images in each well, which were obtained at fixed positions and biased towards the center using the 20x objective. The 20x images were considered technical replicates. Cell counts were determined based on the 5x overview pictures, and analysed in Fiji using a macro for automatic background subtraction, Otsu threshold, watershedding, and particle analysis. The median fluorescence intensity (MFI) for collagen I and III was measured with Fiji based on the 20x close-up images. MFI were used as opposed to mean fluorescence intensity to avoid high intensity areas from affecting the measures disproportionately.

## 7.8 Flow Cytometry

Flowcytometric analyses were performed on a BD FACSLyric Flow Cytometer using a BD FACSuite Application (V1.3.1). As part of the flow cytometer start-up, a preliminary performance quality control was performed using cytometer setup and tracking (CS&T) beads (BD Biosciences, cat. no. 656505) to define the baseline performance of the flow cytometer, including compensation and establishing linearity. All similar analyses were run at fixed voltages, and data was acquired for one minute at medium flow rate. Subsequent data analyses were conducted using FlowLogic (Inivai Technologies Pty. Ltd., FlowLogic v8.7) with identical approaches to grouping data, gating to remove debris, then doublets and lastly, dead cells (Appendices A.5 and A.6 and A.7). From there, the gating strategy varied depending on the desired outcomes of the respective experiments.

Flowcytometric analysis was used to determine optimal PKH26 concentration. The harvested M1:ASC coculture was adjusted to a cell concentration of 1E6 cells/mL and transferred to FACS tubes with 1 mL of FACS buffer, followed by centrifugation and incubation with FVS450 for 15 minutes at RT in the dark. For comparison, cocultures were also labelled with conjugated primary antibodies in FACS buffer: FITC Mouse anti-Human CD90 (1:16) (31.25  $\mu$ g/mL) (BD Biosciences, cat. no. 555595) and PE Mouse anti-human CD45 (1:1) (BD Biosciences, cat. no. 555483) for 30 minutes at RT. Subsequently, they were washed in FACS buffer, before being centrifuged and fixated in 4% paraformaldehyde in PBS for 20 minutes at RT. The cells were then centrifuged, resuspended in 200  $\mu$ L of FACS buffer, and analysed on the flow cytometer. The CD45 antibody staining was not included when ASCs were labelled with PKH26, as both fluoresce in the PE channel. The percentage of macrophages that adsorbed PKH26 dye was investigated with a Boolean gate to exclude CD90-positive cells from the population of viable cells (Appendix A.6E, bottom row).

This procedure was also used for evaluating the separation of the M1:ASC coculture with

Dynabeads by flow cytometry. Unstained controls were included as well as monoculture controls with CD90-labelled ASCs and CD45-labelled macrophages. The percentage of remaining ASCs were determined by plotting both CD45 and CD90 in a CD45 x CD90 plot. Successful separation was defined as the removal of all or most of the ASCs from the sorted macrophage sample, when compared to an unsorted M1:ASC sample.

## 7.9 Statistics

Statistical analyses were performed using SPSS (IBM SPSS Statistics v28.0.1.1(14)). Shapiro Wilks tests of normality were conducted, and nonparametric Kruskal Wallis rank tests were used to evaluate the difference in medians both for the various cell concentrations and conditions, followed by Dunn's test for pairwise comparisons. p-values of 0.05 were considered significant and data is reported as median  $\pm$  standard deviation. The SPSS chart builder was used to illustrate results with subsequent processing in InkScape (Inkscape Developers, v1.0.2-2).

## 8 | Results

### 8.1 Validation of the Macrophage Model

Images were acquired during monocyte differentiation into macrophages (Figure 8.1).

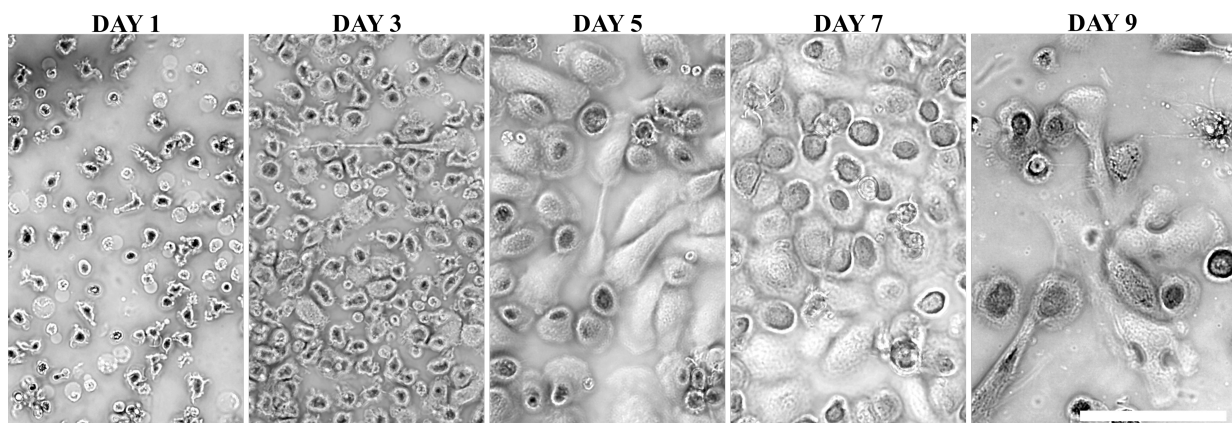


**Figure 8.1: Differentiation of monocytes into macrophages.** Macrophages were differentiated from monocytes using 10 ng/mL GM-CSF over the course of seven days. Images were acquired at day one, three, five, and seven to document the differentiation before coculture with ASCs. The image from day nine shows the macrophage-ASC-coculture with mature macrophages. Scale bar 100  $\mu$ m.

During the differentiation from day one to day seven, the cells grew markedly in size. They also changed their morphology from small, round cells with few protrusions at day one, to large, egg-shaped and adherent cells on day seven. At day nine, after activation with LPS and IFN- $\gamma$  and coculture with ASCs the macrophages appear bigger and more spindle-shaped.

## Optimization of Activating Stimuli

The optimal concentrations of activating stimuli (LPS and IFN- $\gamma$ ) were determined through ELISA analysis of the TNF- $\alpha$  concentration, which was normalised by cell count. Firstly, the proper dilution of samples was determined to be 25x (Appendix A.2). The concentration of TNF- $\alpha$  did not seem to differ based on the presence of ASCs, although increasing concentrations of LPS caused increasing concentrations of TNF- $\alpha$ . Meanwhile, there were no differences in the concentration of TNF- $\alpha$  at different concentrations of IFN- $\gamma$  (Appendix A.3). The inconclusive results prompt the use of 100 ng/mL LPS and 20 ng/mL IFN- $\gamma$ .

## Optimization of PKH26 staining

The optimal concentration of the PKH26 membrane stain was determined with the intention of using PKH26 to evaluate, if the ASCs were phagocytised by the macrophages during the coculture. The ideal concentration of PKH26 was found to be 0.625  $\mu$ M. At this concentration there was a visible difference between stained and unstained cells, and the cell viability was almost at the same level as the Diluent C control (Appendix A.5). However, there was a noticeable difference in cell viability between the Diluent C control and the unstained control, which suggests that many cells perish during the process regardless of PKH26 concentration.

Macrophage uptake of PKH26 dye was evaluated through flowcytometric analysis. Based on labelling with CD90 and CD45 antibodies, it was possible to distinguish between macrophages and ASCs. Furthermore, when using PKH26-labelled ASCs, there was a difference in intensity between CD90-positive and CD90-negative cells, suggesting that these could be separated (Appendix A.6). Around 16% of the mM1 macrophages were PKH26-positive after coculture with PKH26-labelled ASCs, which indicate some phagocytic activity of the macrophages (Appendix A.6E, bottom picture).

## 8.2 Separation of Coculture

In order to utilize the macrophages in later setups, it was necessary to determine whether the M1:ASC coculture could be suspended as single cells. Initial testing of aggregation with a NC-202 suggested that this could be done to a reasonable degree. Additionally, the cell suspension was sorted using MACS, but this resulted in a considerable loss of cells (Appendix A.8). Therefore, the M1:ASC coculture was separated using Dynabeads. A titration of the optimal Dynabead-cell ratio was performed, and the optimal ratio was found to be 20 beads/cell (Appendix A.7).

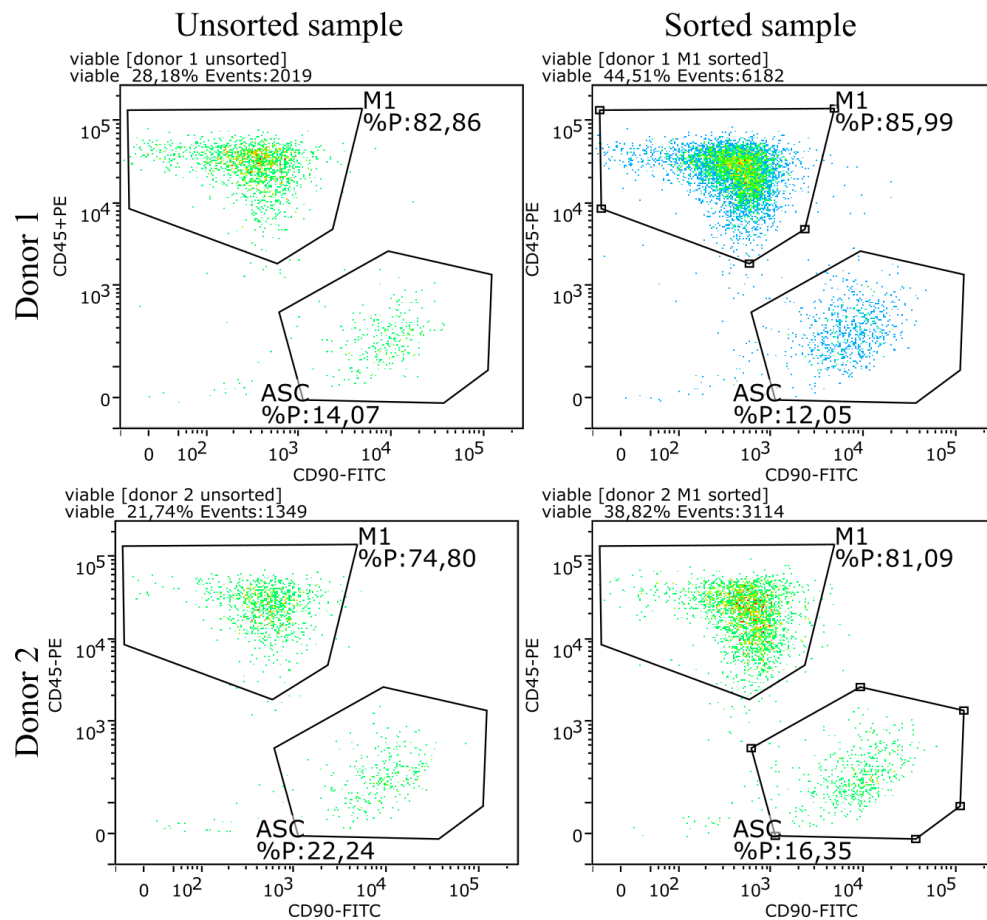


**Figure 8.2: Assessment of the Separation of M1:ASC Coculture using flow cytometry.**

Evaluating the separation of the M1:ASC coculture with Dynabeads based on sorted and unsorted samples from two donors. ASC: adipose-derived stromal cell, M1: M1 macrophage

After separation of the M1:ASC coculture with Dynabeads, the quality of the sorting was tested. For both donor 1 and 2, there was only a small difference in the percentage of remaining ASCs between the sorted (12.1% and 16.4%, respectively) and the unsorted samples (14.1% and 22.2%, respectively) (Figure 8.2). This suggested, that the Dynabeads were not very effective in separating the ASCs from the macrophages.

### 8.3 Determining the Optimal Seeding Density of Fibroblasts

The aim of this study was to determine the optimal seeding density of the fibroblasts, but also to investigate whether removal of TGF- $\beta$  after three days would still result in sufficient deposition of ECM. The optimal seeding density was defined as a cell concentration at which the fibroblasts had room to proliferate, but also had sufficient cell numbers to maintain optimal function.

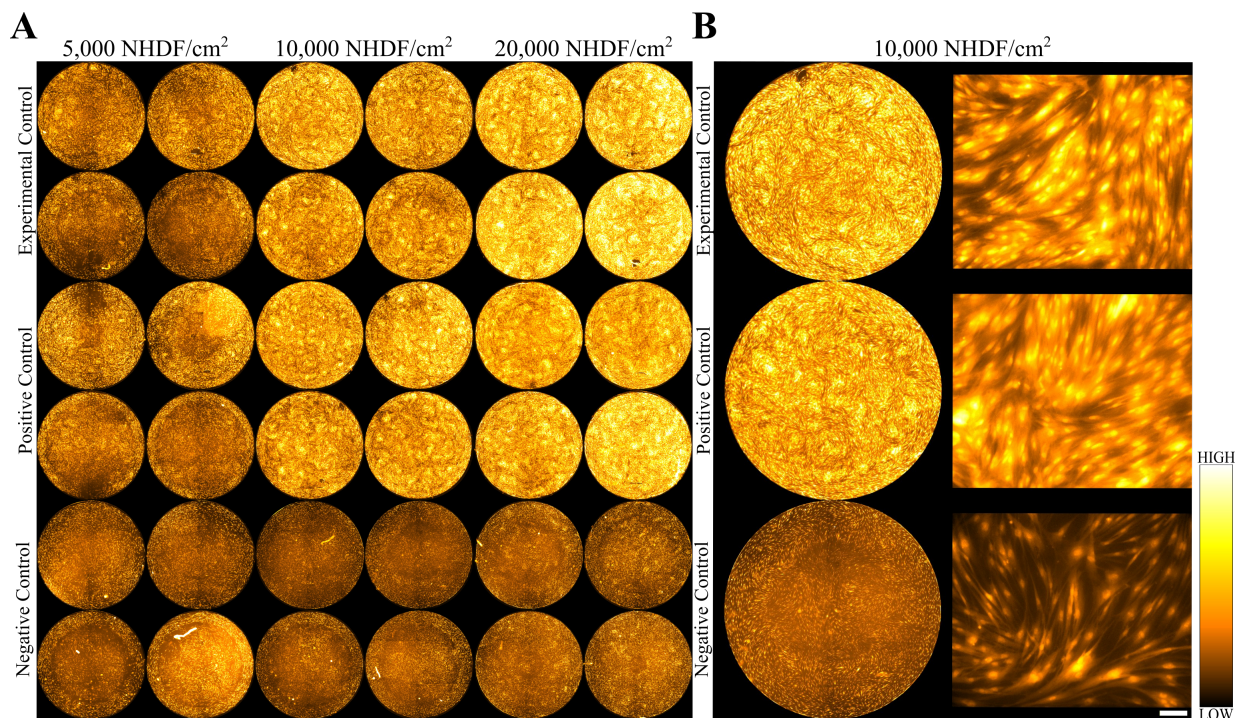


**Figure 8.3:** PicroSirius stained fibroblasts after six days of experimental conditions. A: 5x overview pictures showing staining of fibroblasts in Sirius Red (0.1%) in Picric acid after six days of experimental conditions, with the aim of determining their optimal seeding density. The experimental control was stimulated with TGF- $\beta$  for three days, and then received Ficoll medium for three days. The positive control was stimulated with TGF- $\beta$  for all six days. The negative control was not stimulated with TGF- $\beta$  at any time. B: Comparison of the collagen deposition in the PicroSirius-stained fibroblasts at a seeding density of 10,000 NHDF/cm<sup>2</sup> between the experimental control, the positive control, and the negative control illustrated with both overview and close-up images to highlight collagen localization. Wells are 0.32 cm<sup>2</sup>. Scale is 100  $\mu$ m. NHDF: normal human dermal fibroblast.

There was an obvious visual difference from both the experimental and positive control to the negative control, and also between fibroblast concentrations of 5,000 NHDF/cm<sup>2</sup> to 10,000 and 20,000 NHDF/cm<sup>2</sup> (Figure 8.3A). Both the overview and close-up images for 10,000 NHDF/cm<sup>2</sup> for both experimental, positive, and negative controls illustrated that

collagen was primarily localized inside the cells and around the nuclei. However, both the experimental control and the positive control had some deposition of collagen outside the cells and some visible fibrils (Figure 8.3B).

Comparison between different cell concentrations showed some significant differences across conditions. For the experimental control, significant differences were found when comparing both 20,000 NHDF/cm<sup>2</sup> ( $2880 \pm 325.5$ ) and 10,000 NHDF/cm<sup>2</sup> ( $2081.5 \pm 193.3$ ) to 5,000 NHDF/cm<sup>2</sup> ( $1444 \pm 161$ ). Similarly, the positive control showed significant differences from 20,000 NHDF/cm<sup>2</sup> ( $2622 \pm 347$ ) and 10,000 NHDF/cm<sup>2</sup> ( $2256 \pm 199.5$ ) to 5,000 NHDF/cm<sup>2</sup> ( $1515.5 \pm 215.8$ ). For the negative control, there were significant differences from 20,000 NHDF/cm<sup>2</sup> ( $1307.5 \pm 86.8$ ) to both 10,000 NHDF/cm<sup>2</sup> ( $1204 \pm 60.9$ ) and 5,000 NHDF/cm<sup>2</sup> ( $1217 \pm 198.4$ ) (Figure 8.4).

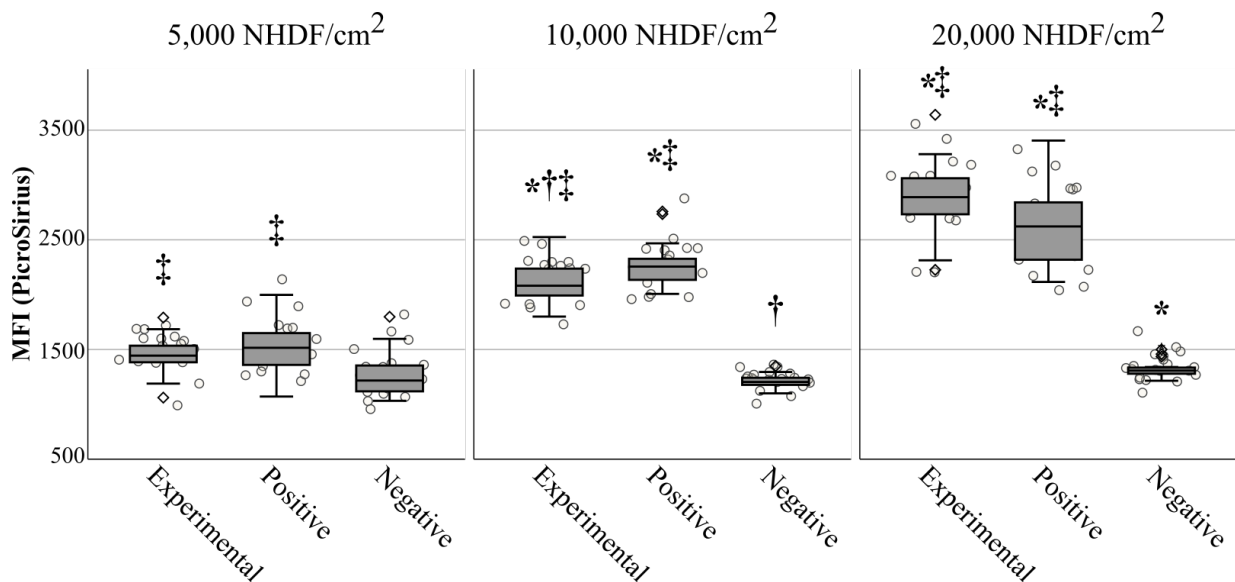


**Figure 8.4: Determining fibroblast seeding density after six days of experimental conditions.** Comparison of MFI based on close-up pictures of PicroSirius-stained fibroblasts seeded at different densities after six days of experimental conditions, between an experimental control and positive and negative controls. Asterisk \* indicates significant difference from 5,000 NHDF/cm<sup>2</sup>. Dagger † indicates significant difference from 20,000 NHDF/cm<sup>2</sup>. Double dagger ‡ indicates significant difference from the negative control. NHDF: normal human dermal fibroblast. PicroSirius: Sirius Red (0.1%) in Picric acid.

Additionally, significant differences were found between both the experimental and negative control, and the positive and negative control at all fibroblast concentrations (Figure 8.4). At all concentrations, the experimental control fibroblasts deposited sufficient amounts of ECM, but 10,000 NHDF/cm<sup>2</sup> was deemed the optimal seeding density, due to a greater difference in MFI from the negative control to the other conditions, and because the data was less dispersed.

## 8.4 Initial Setup of Macrophage and Fibroblast Coculture

To determine the optimal seeding density of the macrophages, differences in MFI of collagen I and collagen III were measured. The optimal seeding density was defined by a great significant and numerical differences in MFI between conditions.

To expose whether any effect on the ECM was caused by excessive cell proliferation, the cell count was determined. The number of cells increased corresponding to increasing seeding density when comparing the ASC-M1 to the fibroblast experimental control. Cell counts for M1:NHDF cocultures with mM1 or imM1 macrophages did not reflect increasing seeding densities as the number of cells dropped at lower concentrations and were increased for higher concentrations (Figure 8.5A). An excerpt illustrating the method for cell counting demonstrated that macrophages were included in the count, and thus the cell count represents the combined number of macrophages and fibroblasts (Figure 8.5B).

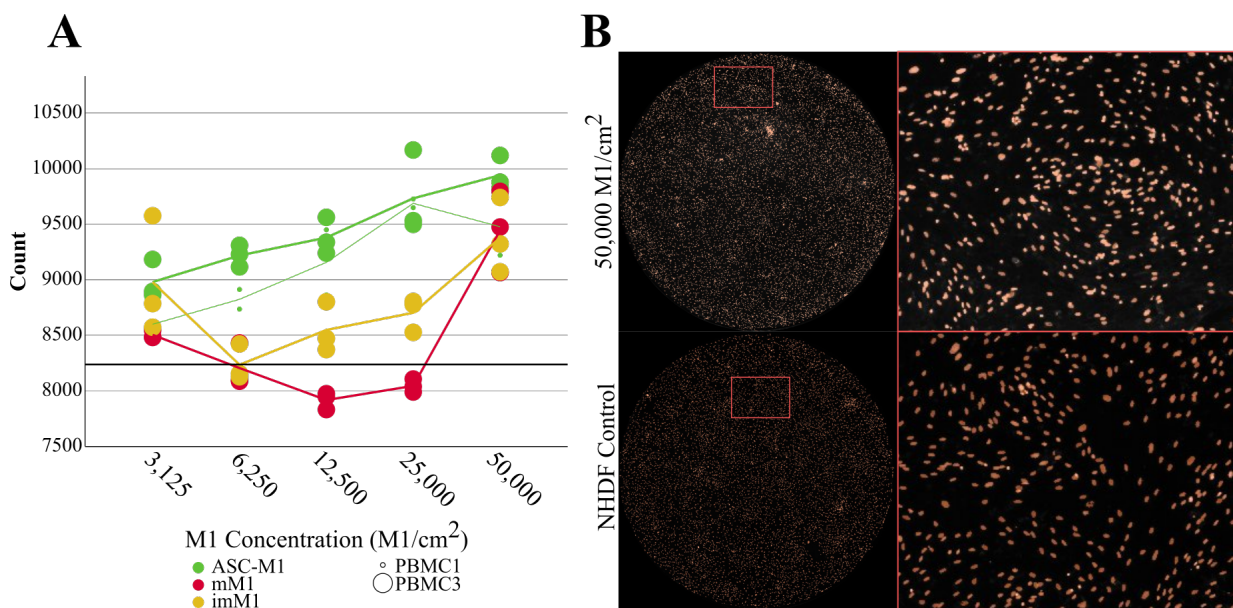


**Figure 8.5: Cell counts of macrophage-fibroblast-cocultures after six days.** A: Cell count of ASC-M1, mM1, and imM1 macrophages based on Hoechst staining of M1:NHDF cocultures. Reference line indicates median for NHDF experimental control, which is considered baseline cell count. B: Cell counting masks based on Hoechst staining of the M1:NHDF cocultures containing 50,000 M1/cm<sup>2</sup> compared to a NHDF experimental control, illustrating the inclusion of macrophages in the count. Red colour indicates a counted cell. ASC: adipose-derived stromal cell, ASC-M1: ASC-treated M1 macrophage, mM1: mature M1 macrophage, imM1: immature M1 macrophage, PBMC: Peripheral blood mononuclear cell, NHDF: normal human dermal fibroblast.

Higher concentrations of ASC-M1 macrophages resulted in decreased levels of collagen I. Significant differences were found at 6,250 M1/cm<sup>2</sup> ( $6726 \pm 307.7$  and  $7084 \pm 245.4$ ),

12,500 M1/cm<sup>2</sup> (6636 ± 185.4 and 7220 ± 288.1), and 50,000 M1/cm<sup>2</sup> (6420 ± 252.1 and 6602 ± 138.6) between ASC-M1 and imM1 macrophages, respectively (Figure 8.6A). Higher concentrations of ASC-M1 led to decreased amounts of collagen III, which was less pronounced than for collagen I, but with significant differences at 6,250 M1/cm<sup>2</sup> (3343 ± 870.6 and 2594 ± 796.7) and 50,000 M1/cm<sup>2</sup> (2709 ± 823.3 and 2233 ± 116.2) between ASC-M1 and the imM1, respectively, and also between the ASC-M1 (3286 ± 1483.6) and the mM1 macrophages (2723 ± 378.9) at 12,500 M1/cm<sup>2</sup>.

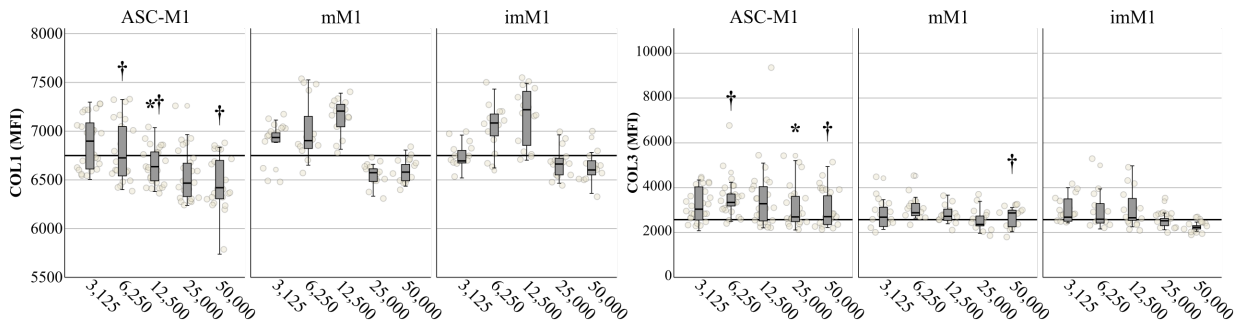


**Figure 8.6: Comparison of collagen deposition at different concentrations of M1 after six days.** There were no great differences between the MFI of collagen I or III at different concentrations of macrophages or different conditions based on antibody staining of collagen I and III after six days. Reference line indicates median for the fibroblast experimental control. Asterisk \* indicates significant difference from mM1. Dagger † indicates significant difference from imM1. COL1: collagen I, COL3: collagen III, MFI: median fluorescence intensity, ASC-M1: ASC-treated M1 macrophage, mM1: mature M1 macrophage, imM1: immature M1 macrophage

The levels of collagen across all macrophage conditions were very close to those produced by the fibroblast control for both collagen I (6670.5 ± 202.7) and collagen III (2575.1 ± 577.1), and while it seemed that the ASC-M1 were able to slightly reduce collagen I, overall the results were inconclusive in terms of deciding optimal seeding density of the macrophages (Figure 8.6B).

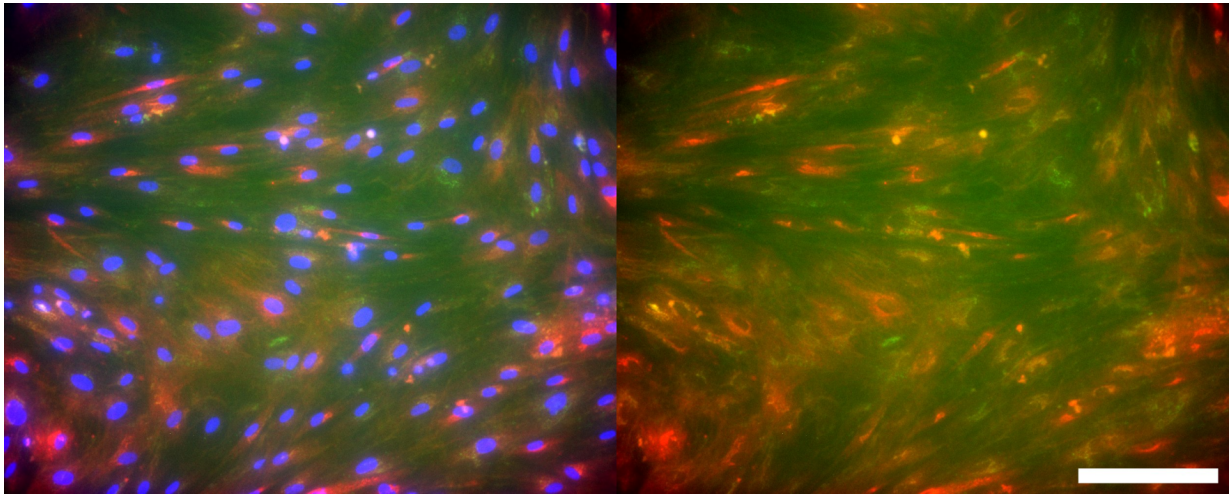


**Figure 8.7: Organization of collagen after three days of macrophage-fibroblast-coculture.**

Example of image with ASC-M1 seeded at  $6250 \text{ M1/cm}^2$ , stained with Hoechst 33343, and anti-collagen I and anti-collagen III antibodies after six days. This illustrates the location of collagen I (green) and collagen III (red) around the nuclei of the fibroblasts (blue). Nuclei are removed on right picture. Scale  $100 \mu\text{m}$ .

Both collagen I and collagen III were primarily localised inside the cells, placed densely around the nuclei, and with almost no visible collagen fibrils outside the cells (Figure 8.7). When compared to the collagen organization seen when determining fibroblast seeding density (Figure 8.3B) the potential benefit of extending the study was substantiated, as it would allow for more deposition of ECM.

## 8.5 Determining Optimal Seeding Density of Macrophages in an Extended Setup

The aims were to determine the optimal seeding density of macrophages in the extended study setup, and to evaluate the influence of macrophage activation on the ECM compared to that of the ASC-M1 macrophages.

At first, the effect of the extended setup was determined. Significant differences in collagen deposition were found in the levels of collagen I between experimental controls on day six ( $1019 \pm 64.8$ ) and day nine ( $2182 \pm 429$ ) (Figure 8.8A) and in collagen III between the positive controls and negative controls on day six ( $954 \pm 116.1$  and  $1011 \pm 217.1$ , respectively) and day nine ( $988.5 \pm 74.6$  and  $871 \pm 84.5$ , respectively) (Figure 8.8B).

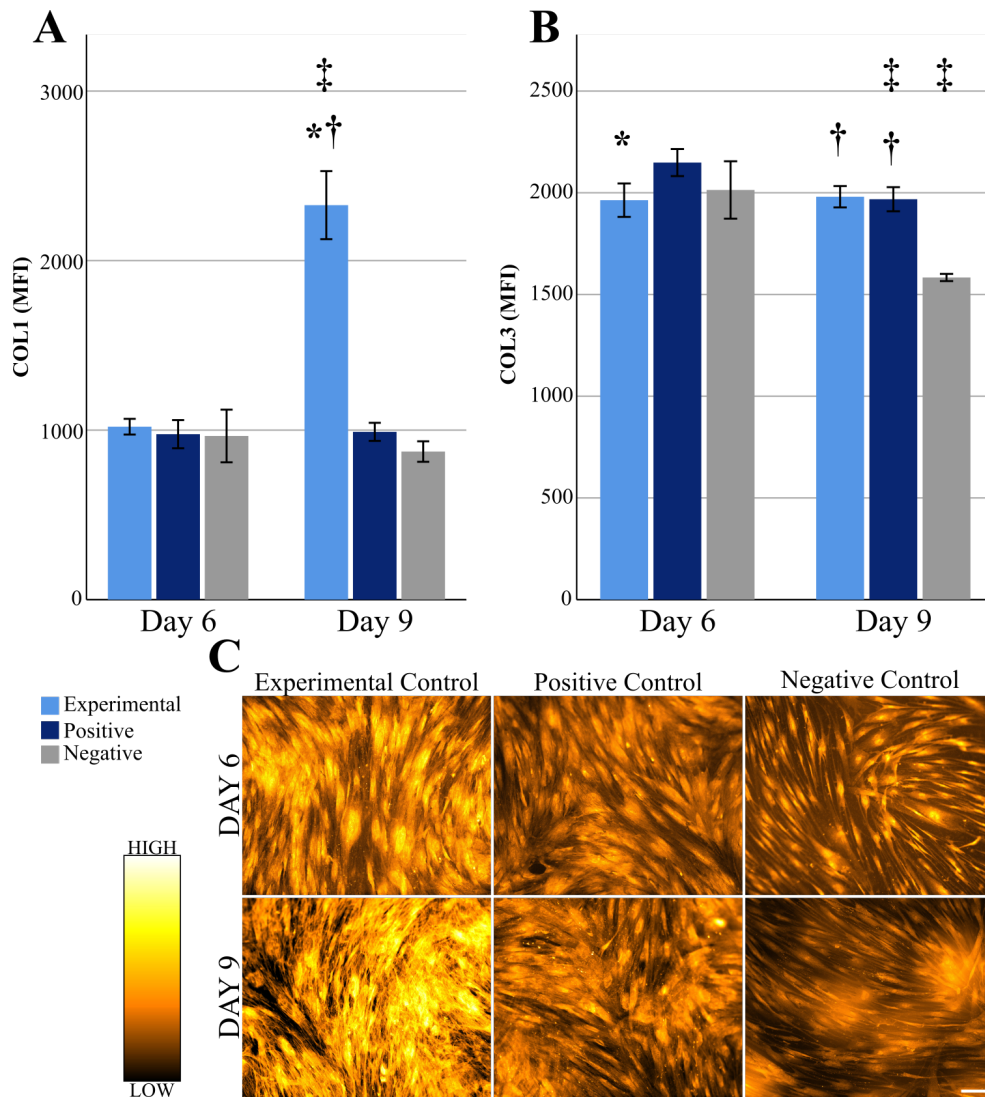


**Figure 8.8: Differences in deposition of collagen I and III from fibroblasts between six and nine days.** Comparison of MFI for collagen I (A) and collagen III (B) from day six to day nine for fibroblast control groups based on antibody staining of collagen I and III. Asterisk \* indicates significant difference from the positive control. Dagger † indicates significant difference from the negative control. Double dagger ‡ indicates significant difference from day six. C: Comparison of collagen organization from day six to day nine across conditions based on staining of fibroblasts with Sirius Red (0.1%) in Picric acid. Scale 100  $\mu$ m. MFI: median fluorescence intensity, COL1: collagen I, COL3: collagen III.

At day six, most of the collagen fibers were located inside the fibroblasts and around the nuclei as opposed to forming an extracellular fibril-dense mesh (Figure 8.8C, top row). On day nine, a more pronounced ECM-like structure was formed, and the fibers were not confined within the cells, especially for the experimental control (Figure 8.8C, bottom row). Significant differences between groups were found in collagen I between the experimental control and both the positive and negative control (Figure 8.8A). Consequently, this sug-

gests that the additional three days allowed for more deposition of ECM, and also for the macrophages to affect the deposition of collagens more.

The total number of cells were determined in order to establish that any effect was due to the function of the macrophages, and not to any presence of ASCs or excessive proliferation.

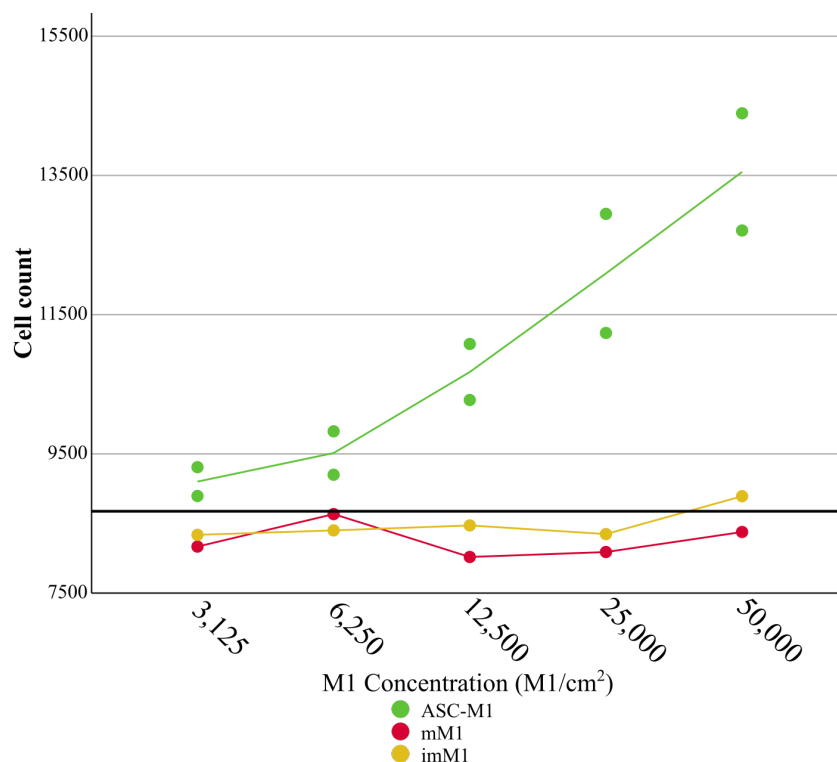


**Figure 8.9: Cell count in macrophage-fibroblast-cocultures after nine days.** Cell count based on Hoechst stained overview images of M1:NHDF and fibroblast experimental controls after nine days. Reference line indicates median for NHDF experimental control, which is considered the baseline cell count. ASC: Adipose-derived stromal cell, ASC-M1: ASC-treated M1 macrophage, mM1: mature M1 macrophage, imM1: immature M1 macrophage.

The number of ASC-M1 macrophages rose proportionally to increasing M1 concentration, while numbers of mM1 and imM1 macrophages were steady at baseline, indicating that only fibroblasts were present (Figure 8.9). The method used to determine the cell count was identical to that of the six-day-setup, therefore this cell count was deemed representative of the total number of both macrophages and fibroblasts (Figure 8.5B). The cell viability for the harvested M1:ASC coculture was lower than for the mM1 and imM1 macrophages, indicating that coculture with ASCs caused more macrophages to die compared to monocultured macrophages (Appendix A.9).

The optimal concentration of macrophages was defined as a concentration with significant difference between ASC-M1 and mM1 macrophages, which applies to both collagen I and III

at all concentrations. The imM1 macrophages were included to evaluate whether activation of macrophages was necessary to induce an effect on the ECM. The imM1 macrophages resulted in lower levels of both collagen I and collagen III compared to the mM1, indicating that the macrophages need to be activated, for them to have an effect on the ECM (Figures 8.10A and B).

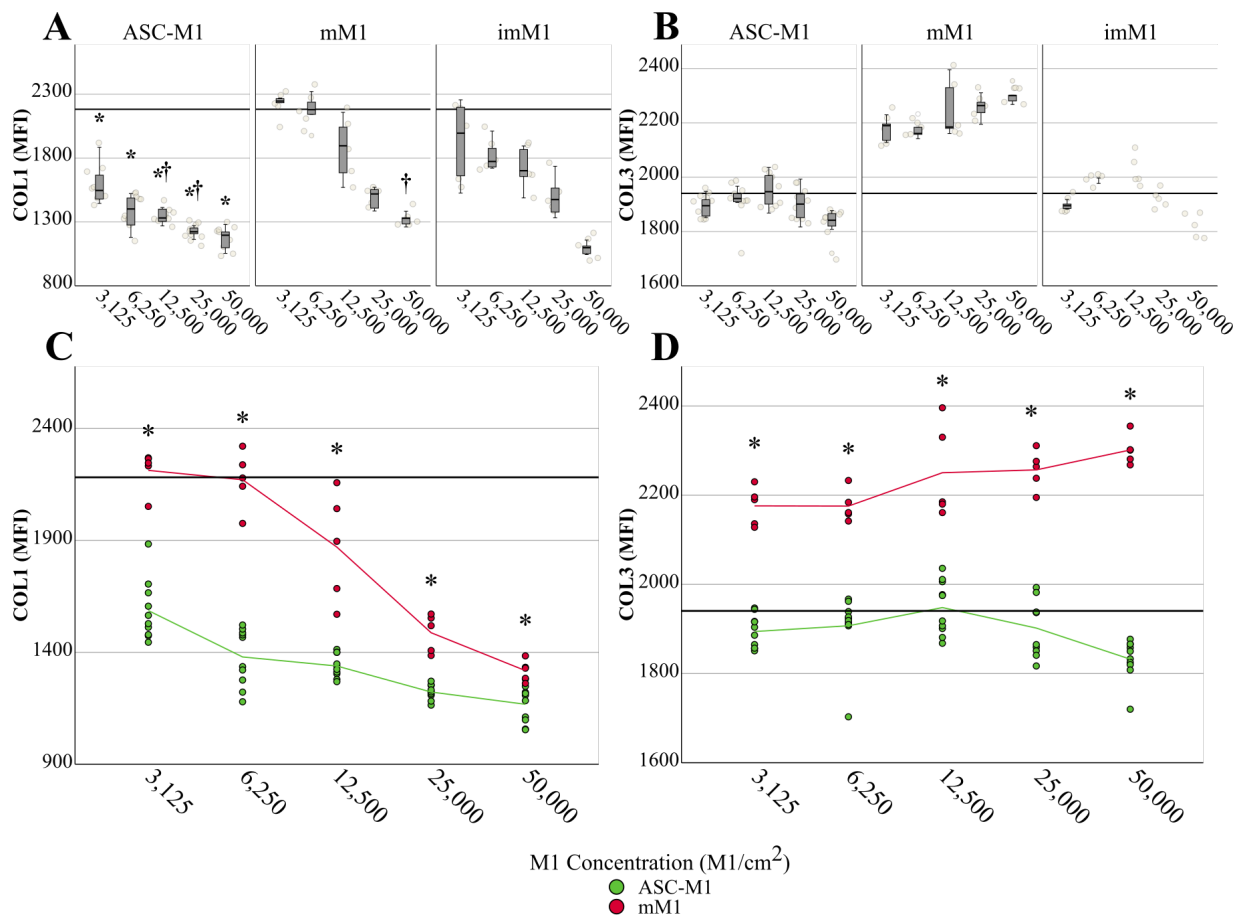


**Figure 8.10: Comparison of collagen deposition at different concentrations of M1 after nine days.** Comparison of MFI for collagen I (A) and collagen III (B) for M1 concentrations across conditions. MFI for collagen I (C) and collagen III (D) is used to illustrate the numerical difference between ASC-M1 and mM1. MFI is measured based on antibody staining of collagen I and III. Reference line indicates median of NHDF experimental control. Asterisk \* illustrates significant difference from mM1. Dagger † illustrates significant difference from imM1. COL1: collagen I, COL3: collagen III, MFI: median fluorescence intensity, ASC: Adipose-derived stromal cell, ASC-M1: ASC-treated M1 macrophage, mM1: mature M1 macrophage, imM1: immature M1 macrophage.

Higher concentrations of macrophages resulted in lower levels of collagen I, and significant differences were found at concentrations of 3,125 M1/cm<sup>2</sup> (1546.5 ± 134.5 and 2246 ± 91.2), 6,250 M1/cm<sup>2</sup> (1401.5 ± 127.3 and 2179 ± 128.4), 12,500 M1/cm<sup>2</sup> (1331 ± 51.3 and 1896 ± 243.6), 25,000 M1/cm<sup>2</sup> (1223 ± 32.8 and 1519 ± 85), and 50,000 M1/cm<sup>2</sup> (1196

$\pm 81.2$  and  $1329 \pm 47.7$ ) between the ASC-M1 and the mM1 macrophages, respectively (Figure 8.10C). In general, the levels of collagen I were lower compared to the fibroblast control ( $2182 \pm 429$ ) for both ASC-M1 and mM1 macrophages. The levels of collagen III were similar between ASC-M1 macrophages and the fibroblast control ( $1940.5 \pm 112.1$ ), but elevated for the mM1 macrophages. While the ASC-M1 macrophages resulted in lower levels of collagen III than the mM1, the difference between ASC-M1 and the mM1 did not vary much between the different concentrations (Figure 8.10D).

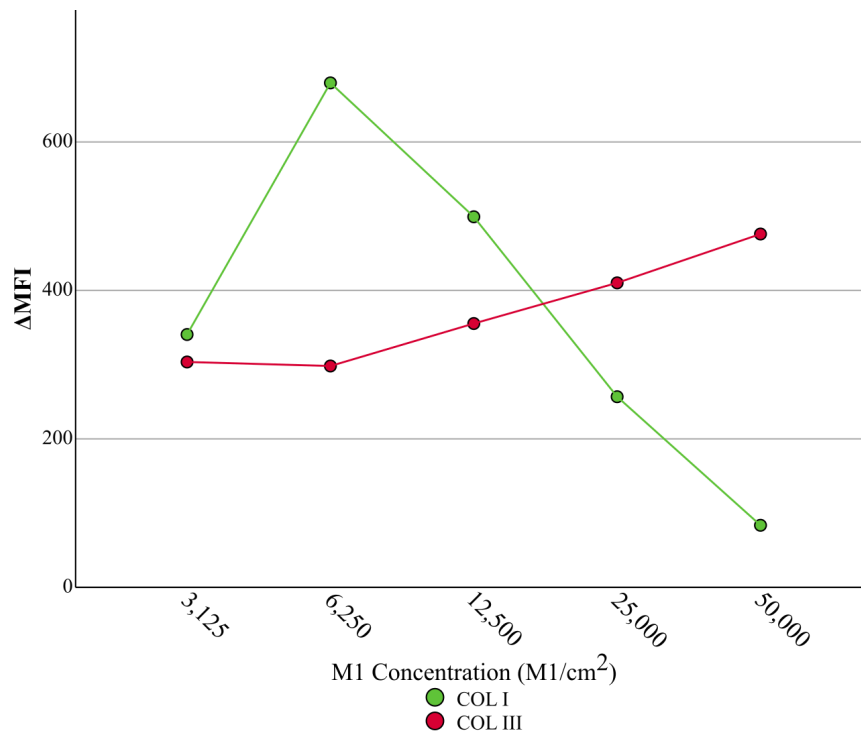


**Figure 8.11: Numerical differences in MFI between mM1 and ASC-M1.** The exact numerical differences in MFI from mM1 to ASC-M1 can be calculated as the delta ( $\Delta$ )-value. Green line indicates collagen I. Red line indicates collagen III. ASC: Adipose-derived stromal cell, ASC-M1: ASC-treated M1 macrophage, mM1: mature M1 macrophage, mM1: immature M1 macrophage.

The greatest numerical difference for both collagen I and collagen III can be seen at 6,250 M1/cm<sup>2</sup> (Figure 8.11). Therefore this concentration appears to be the optimal concentration at which the macrophages are able to elicit an effect on the ECM.

## 9 | Discussion

In order to establish a coculture model of mM1 macrophages and ASCs, the optimal concentration of LPS and IFN- $\gamma$  was determined. The phenotype of macrophages were confirmed based on their morphology through microscopic analysis during the differentiation process. We found that increasing concentrations of LPS resulted in elevated concentrations of TNF- $\alpha$ , suggesting some dependence between the LPS stimuli and the production of TNF- $\alpha$ . However, as all concentrations resulted in similar levels of TNF- $\alpha$ , it was not possible to further pinpoint the optimal concentration of activating stimuli. Therefore, concentrations of 100 ng/mL LPS and 20 ng/mL IFN- $\gamma$  were deemed optimal. This was in concordance with other studies, who have used 100 ng/mL LPS and 20 ng/mL IFN- $\gamma$  as activating stimuli to induce mM1 macrophages (Jaguin et al., 2013; Holthaus et al., 2022). Furthermore, Holthaus et al. (2022) and Jaguin et al. (2013) confirmed the phenotype of the mM1 macrophages by their spindle-shaped appearance, and by measuring an increased secretion of TNF- $\alpha$  and IL-10. As TNF- $\alpha$  is a pro-inflammatory cytokine, and typically secreted by mM1 macrophages, the expression of TNF- $\alpha$  was expected to decrease after coculture with ASCs, as these have been shown to promote a phenotypic change in macrophages (Stevens et al., 2020). Based on this, there is reason to believe that we did in fact induce mM1 macrophages, but it could have been investigated further, e.g. through analysis of the expression of surface markers. While our focus was to develop a coculture model with mM1 macrophages, it could be interesting to include mM2 macrophages for comparison with the ASC-M1 macrophages.

To investigate the cell-cell contact dependent interactions between ASCs and macrophages, we explored PKH26-labelling of the ASCs to measure their uptake by macrophages. After coculture, only a small amount of macrophages were found to be PKH26-positive, suggesting that few ASCs were phagocytised by macrophages. It should be noted, that the concentration of PKH26 was optimized to provide a strong signal while retaining high viability of the ASCs, and it was not investigated how uptake of PKH26 affected the function of the macrophages. Still, the viability of the PKH26-labelled ASCs were decreased when compared to an unstained control. Labelling of ASCs with PKH26 has been used as a measure of macrophage phagocytosis in other studies, and while further optimisation is needed, the method shows promise. Braza et al. (2016) showed that ingestion of PKH26-labelled MSCs by macrophages caused them to upregulate their expression of TGF- $\beta$  and

IL-10 compared to PKH26-negative macrophages. Similarly, de Witte et al. (2018) showed that PKH26-labelled MSCs were actively phagocytosed by monocytes, resulting in them acquiring an anti-inflammatory phenotype with increased expression of TGF- $\beta$  and IL-10 after three days of coculture with MSCs. This was not in concordance with our study, in which we did not find great phagocytic activity of the macrophages after two days of coculture with ASCs. However, the observation in our study was based on a single event and was not optimised with regard to macrophage function. In order to prevent cell death, we used a lower concentration of PKH26 than Braza et al. (2016) and de Witte et al. (2018), which may have resulted in a weaker signal when the PKH26-labelled ASCs were phagocytised by the macrophages. This implies, that even if the macrophages ingested PKH26 the resulting signal may have been below the detection limit. Further research is needed to definitively comment on the macrophage-ASC-interaction based on PKH26 membrane labelling.

In addition to cell-cell dependent interactions, the ASCs are known to exert their effects through paracrine secretions that lead to activation of immune cells and repolarisation of macrophages, which in turn can promote tissue regeneration (Bian et al., 2022). de Witte et al. (2018) and Holthaus et al. (2022) found that mM1 macrophages acquired an anti-inflammatory phenotype when in the presence of MSCs, but also when treated with conditioned medium from MSCs. Interestingly, Braza et al. (2016) found that the level of TNF- $\alpha$  did not change based on macrophage phenotype. This suggests, that it might not be suitable to detect changes in macrophage phenotype, and thus other markers such as TGF- $\beta$  or IL-10, which have been shown to induce a change in expression patterns by e. g. de Witte et al. (2018) and Holthaus et al. (2022), could be used instead. Both TGF- $\beta$  and IL-10 are anti-inflammatory markers typical for mM2 macrophages, and an increased expression of these markers indicate that MSCs are able to polarise mM1 macrophages towards an mM2 phenotype. As such, the presence of either MSCs or MSC-fragments may promote repolarisation of macrophages from an mM1 to an mM2 phenotype, and it seems that both cell-cell dependent interactions, as well as the paracrine secretions are important for the macrophage-ASC-interactions. It should be noted, that mM2 macrophages tend to have a higher phagocytic activity than mM1 macrophages and in addition, the phagocytic activity of macrophages in itself promotes the mM2 phenotype (Shapouri-Moghaddam et al., 2018). Based on this, it would be interesting to investigate the effect of the ASCs on the expression profile of the macrophages.

In order to utilize the macrophages in the ECM model, the macrophage-ASC-coculture had to be separated. Due to an inefficient separation by Dynabeads, all ASCs were not removed. This suggests that the method needs to be modified, for example by further optimizing the use of CD90-coated Dynabeads or by choosing alternative methods altogether. Data obtained through flowcytometric analysis using CD45 and CD90 antibodies suggests that separation with fluorescence-activated cell sorting (FACS) would result in a more pure macrophage population. However, this method is not ideal either, as it is time-consuming and many cells tend to be lost during the process.

To determine if the coculture with ASCs had an effect on macrophage polarisation, the effect of ASC-M1 macrophages were compared to mM1 macrophages. The mM1 macrophages were found to induce a smaller effect on the ECM than the ASC-M1, which was illustrated by a smaller decrease in the levels of collagen. This may be due to their polarisation state, which refers to the phenotype of the macrophages, i.e. whether they are mM1- or mM2-like macrophages. Furthermore, the differences between the mM1 and the imM1 macrophages indicate that activation of macrophages increase their effect on the ECM. A study by Zhou et al. (2015) found that functional THP1-derived mM1 macrophages had reduced secretion of TNF- $\alpha$  when seeded in a migration chamber with fibroblasts. They also found that an inflammatory environment had an impact on both macrophages and fibroblasts. This was opposed to an IL-4-rich environment that had no effect on the fibroblasts, but could polarise macrophages towards an mM2 phenotype, which in turn affected the fibroblasts. This emphasises that the polarisation state is important for the type of response observed. The mM1 phenotype has been associated with progression of fibrosis due to release of pro-fibrotic factors such as TGF- $\beta$ , which promotes differentiation of myofibroblasts (Setten et al., 2022). However, the results from both our study and the study by Zhou et al. (2015) indicate that the macrophage-fibroblast interaction is also dependent on the surrounding environment, and suggest that mM1 macrophages in a coculture with fibroblasts are re-polarised to promote an anti-inflammatory environment, similar to the effect of M1:ASC coculture. Consequently, both the ASC-M1 and the mM1 macrophages contribute to the initiation of an anti-inflammatory environment, and as such the amelioration of fibrosis (Zhou et al., 2015).

Differences between the ASC-M1 and the mM1 macrophages may be explained by differences in the exposure of macrophages to ASCs. After harvesting the M1:ASC coculture, the viability of the ASC-M1 macrophages dropped compared to both mM1 and imM1 macrophages. During M1:NHDF coculture, both mM1 and imM1 vanished almost completely, but still had an effect on the ECM similar to that of the ASC-M1 macrophages, although to a lesser extent. A theory could be, that only macrophages that were viable in the ASC-created environment were transferred to the M1:NHDF coculture, and thus were better suited for survival in the fibroblast-created environment. Meanwhile, the mM1 and imM1 macrophages that had not been in a coculture with ASCs did not fare so well. A feasible assumption could be, that the ASC-M1 macrophages that were already activated and polarised by the ASCs, were better equipped to exert an effect on the ECM than the mM1 or imM1 macrophages. The mM1 macrophages were already activated, but before an effect could be seen on the ECM, they needed to be polarised. Similarly, the imM1 macrophages had to be both activated and polarised and were therefore slower to elicit a noticeable effect.

Based on a study by Søndergaard et al. (2022), the setup of the M1:NHDF coculture was extended from six to nine days, to accommodate an increased production of collagen and provide more time for the macrophages to elicit their effect(s). Different seeding densities of the macrophages were tested, and a seeding density of 6,250 M1/cm<sup>2</sup> was chosen, as it induced the greatest significant and numerical difference in collagen levels between

the ASC-M1 and the mM1 macrophages. Other studies have, like us, investigated the macrophage-fibroblast interactions using coculture models, such as Zhao et al. (2022) who found a macrophage-fibroblast ratio of 1:5.3 to be sufficient to induce an effect in a migration chamber, and Setten et al. (2022) who preferred a macrophage-fibroblast ratio of 2:1. Compared to these studies, we used a macrophage-fibroblast ratio of 1:1.6. Neither of the studies used TGF- $\beta$  to stimulate ECM production of the fibroblasts, as we did, and therefore the fibroblasts will likely not produce ECM in the same amount or characteristic. For these reasons, their preferred macrophage-to-fibroblasts ratios may not apply to a model using TGF- $\beta$ -stimulated fibroblasts. Therefore, it was important to identify a macrophage concentration that were suitable in this assay, and resulted in a great numerical difference as well as a significant difference in the levels of collagen, to ensure that it was detectable in all conditions.

The low rate of separation by the Dynabeads resulted in the presence of some ASCs in the M1:NHDF coculture. We did not further explore whether this had any effect on the M1:NHDF coculture. A study by Søndergaard et al. (2022) found that ASCs in coculture with fibroblasts resulted in increased formation of both collagen I and collagen III, suggesting that ASCs were able to promote fibroblast function. Meanwhile, Caires et al. (2018) showed that the presence of MSCs in a macrophage-fibroblast-MS model seeded on chitosan scaffolds could impede fibroblast migration, thereby promoting an anti-inflammatory environment, since increased recruitment of fibroblasts is associated with inflammation. Furthermore, MSCs are known to be able to ameliorate fibrotic disease by modulating macrophage response and improving cell proliferation, but at the same time, exposure to chronic inflammation may cause resident MSCs to engage in formation of myofibroblasts, which consequently lead to progression of fibrosis (Agha et al., 2017; Guillamat-Prats, 2021). This suggests, that the ASCs affected the M1:NHDF coculture, and although the exact interactions are unknown, they may have promoted the function of both fibroblasts and macrophages. The exact implications of this could be explored by including ASCs in coculture with macrophages and fibroblasts, to explore the combined interactions between the three cell types, as well as their contribution to tissue regeneration, compared to a coculture of fibroblasts and ASC-treated macrophages.

To determine the feasibility of detecting changes in the type of collagen deposited we used ICC to evaluate the MFI of collagen I and collagen III. We found that the levels of collagen III were upregulated in the presence of mM1 macrophages compared to the effect of ASC-M1 macrophages and to fibroblasts alone. However, while there were differences between collagen I and collagen III, no discernible trend was found. In tissue repair, a granulation tissue rich in collagen III is formed, and as the new tissue regains strength and flexibility it is remodeled to collagen I (Bian et al., 2022). It is possible that the reorganization of the ECM happens over a longer period of time, and is affected by multiple factors in the tissue, and therefore could not be measured in this study. Additionally, both collagen I and collagen III are upregulated in fibrosis and contributes to increased stiffness of the ECM (Zhao et al., 2022). Changes to the ECM may cause different macrophage responses by promoting fibrosis in a positive feedback loop and/or through release of ma-

tricyptins from the ECM, which can affect the interactions between the macrophages and the surrounding environment (Zhao et al., 2022). As such, the remodelling of collagen III to collagen I might not take place in a fibrotic environment, and this may be another reason, it could not be measured in this study. To substantiate the interactions between macrophages and fibroblasts, other markers could have been included, for example fibronectin, which is a regulator of collagen organization. Fibronectin is predominantly secreted by fibroblasts and stromal cells, but monocytes have also been shown to produce fibronectin in a pro-inflammatory environment, where increased deposition of fibronectin has been linked to fibrotic conditions (Vasse et al., 2021).

Macrophages are involved in the maintenance of the ECM through secretion of MMPs, which enables them to regulate degradation and deposition of ECM (Zhao et al., 2022). The secretion of MMPs by macrophages could be measured in a protein analysis assay such as ELISA or western blot, and used to provide an insight into the function of macrophages in the ECM. Additionally, the expression profiles of MMPs in the macrophages could have been investigated with quantitative Polymerase Chain Reaction (qPCR) to discover any changes in the protein expression profile of the macrophages.

Due to the presence of both macrophages and fibroblasts in our ECM model, it is difficult to discern between effects that are caused by macrophage-fibroblast versus macrophage-ECM interactions. This raises the question of whether these interactions are inevitably linked, or if the macrophages would have an effect even without any fibroblasts present. It could be investigated by decellularising the ECM prior to addition of macrophages, which would provide an isolated picture of the macrophage-ECM interactions. Alternatively, an inhibition assay could be performed to ensure that the effect on the ECM is in fact caused by macrophage function and/or macrophage-fibroblast interactions by administration of a fibroblast inhibitor, e.g. Osthole. Osthole is a coumarin-derivative that has been shown to suppress activation and proliferation of both fibroblasts and myofibroblasts with subsequent reduction of fibrosis even in the presence of TGF- $\beta$  (Zhang et al., 2018).

To investigate the amount of collagen in the ECM, a collagen quantification assay could have been a more precise method compared to determining the MFI through fluorescent microscopy. Examples of quantification assays are colorimetric assays, such as a hydroxyproline assay (Abcam, 2023) or staining with Sirius Red/Fast Green (Chondrex, 2020). In both, the optical density is measured using a plate reader, and used to determine the amount of collagen relative to a range of standards. However, we found that PicroSirius also stained macrophages vividly (Appendix A.10). As such, they may fluoresce more than the underlying ECM or the fibroblasts, which is also the reason we did not use PicroSirius to stain the M1:NHDF cocultures. It is uncertain whether the staining of macrophages with PicroSirius is due to unspecific staining or because the macrophages contain and/or produce collagens, which would also contribute to a hydroxyproline assay. In a study by Myllylä and Seppä (1979), macrophages were found to have a small but significant production of hydroxyproline, and another study by Schnoor et al. (2008) found that macrophages produce both collagen VI and collagen VIII. The macrophages use the produced collagen to modulate their binding properties, as they do not produce the proteins required for

aggregation of the collagen filaments (Schnoor et al., 2008). This further complicates the interpretation of the macrophage-fibroblast interaction and in addition, it establishes the importance of including controls with monocultured macrophages and fibroblasts for comparison.

In this study, we have begun to investigate the effect of the ASCs on macrophages as well as their fibrotic effects. These initial experiments are important for establishing modes of actions that can be used in future development of potency assays, which are needed to ensure the quality of ASCs as a cellular therapy product. As of now, the complexity of both the macrophage-ASC-coculture model and the ECM model limit their use as potency assays, but hopefully they can be used in the discovery of relevant biological interactions and/or mechanisms of action of the ASCs. Such discoveries may ensue identification of distinct biomarkers or pathways that can be used to develop suitable potency assays.

## 9.1 Conclusion

We were successful in establishing optimal concentrations of LPS and IFN- $\gamma$  to activate a coculture with macrophages and ASCs. Furthermore, when adding ASC-M1 macrophages to an ECM derived from TGF- $\beta$ -stimulated fibroblasts, the levels of collagen type I and III were decreased, when compared to both a mature macrophage control and to an ECM without macrophages.

In the future, it could be relevant to include additional steps to determine the macrophage phenotype after treatment with ASCs. Additionally, inclusion of assays that more accurately quantifies the amount of collagen in the fibroblast-derived ECM could constitute a more solid outcome for evaluating the fibrotic effect of macrophages.

## 10 | Bibliography

- Abcam. Hydroxyproline assay kit (colorimetric) (ab222941), 2023. URL <https://www.abcam.com/products/assay-kits/hydroxyproline-assay-kit-colorimetric-ab222941.html>.
- R. Agger, C. H. Nielsen, G. Leslie, and B. Aasted. *Immunologi*. Munksgaard, 2015.
- E. E. Agha, R. Kramann, R. K. Schneider, X. Li, W. Seeger, B. D. Humphreys, and S. Bellusci. Mesenchymal stem cells in fibrotic disease. *Cell Stem Cell*, 3;21(2):166–177, 2017. doi: 10.1016/j.stem.2017.07.011. URL <https://pubmed.ncbi.nlm.nih.gov/28777943/>.
- D. Bian, Y. Wu, G. Song, R. Azizi, and A. Zamani. The application of mesenchymal stromal cells (mscs) and their derivative exosome in skin wound healing: a comprehensive review. *Stem Cell Res Ther.*, 13(1):24, 2022. doi: 10.1186/s13287-021-02697-9. URL <https://pubmed.ncbi.nlm.nih.gov/35073970/>.
- P. Bourin, B. A. Bunnell, L. Casteilla, M. Dominici, A. J. Katz, K. L. March, H. Redl, J. P. Rubin, K. Yoshimura, and J. M. Gimble. Stromal cells from the adipose tissue-derived stromal vascular fraction and culture expanded adipose tissue-derived stromal/stem cells: a joint statement of the international federation for adipose therapeutics and science (ifats) and the international society for cellular therapy (isct). *Cytotherapy*, 15:641–648, 2013. doi: <https://doi.org/10.1016/j.jcyt.2013.02.006>. URL [https://www.isct-cytotherapy.org/article/S1465-3249\(13\)00387-3/fulltext](https://www.isct-cytotherapy.org/article/S1465-3249(13)00387-3/fulltext).
- C. A. Bravery, J. Carmen, T. Fong, W. Oprea, K. H. Hoogendoorn, J. Woda, S. R. Burger, J. A. Rowley, M. L. Bonyhadi, and W. V. Hof. Potency assay development for cellular therapy products: an isct\* review of the requirements and experiences in the industry. *Cytotherapy*, 15:9–19, 2013. doi: 10.1016/j.jcyt.2012.10.008. URL <https://pubmed.ncbi.nlm.nih.gov/23260082/>.
- F. Braza, S. Dirou, V. Forest, V. Sauzeau, D. Hassoun, J. Chesné, M. Cheminant-Muller, C. Sagan, A. Magnan, and P. Lemarchand. Mesenchymal stem cells induce suppressive macrophages through phagocytosis in a mouse model of asthma. *Stem Cells*, 34(7): 1836–1845, 2016. doi: 10.1002/stem.2344. URL <https://pubmed.ncbi.nlm.nih.gov/26891455/>.

- H. R. Caires, P. B. da Silva, M. A. Barbosa, and C. R. Almeida. A co-culture system with three different primary human cell populations reveals that biomaterials and msc modulate macrophage-driven fibroblast recruitment. *Journal of Tissue Engineering and Regenerative Medicine*, 12:1433–1440, 2018. doi: 10.1002/term.2560. URL <https://pubmed.ncbi.nlm.nih.gov/28865088/>.
- C. X. C. Chen, Y. X. Peng, X. B. Wang, P. V. Fish, J. L. Kaar, R. R. Koepsel, A. J. Russell, R. R. Lareu, and M. Raghunath. The scar-in-a-jar: studying potential antifibrotic compounds from the epigenetic to extracellular level in a single well. *British Journal of Pharmacology*, 158:1196–1209, 2009. doi: <https://doi.org/10.1111/j.1476-5381.2009.00387.x>. URL <https://pubmed.ncbi.nlm.nih.gov/19785660/>.
- Chondrex. Sirius red/fast green collagen staining kit (9040), 2020. URL <https://www.chondrex.com/products/sirius-red-fast-green-collagen-staining-kit>.
- A. Das, M. Sinha, S. Datta, M. Abas, S. Chaffee, C. K. Sen, and S. Roy. Monocyte and macrophage plasticity in tissue repair and regeneration. *Am J Pathol*, 185(10):2596/2606, 2015. doi: 10.1016/j.ajpath.2015.06.001. URL <https://www.ncbi.nlm.nih.gov/pmc/articles/PMC4607753/>.
- S. de Witte, F. Luk, J. M. S. Parraga, M. Gargasha, A. Merino, S. S. Korevaar, A. S. Shankar, L. O’Flynn, S. J. Elliman, D. Roy, M. G. Betjes, P. N. Newsome, C. C. Baan, and M. J. Hoogduijn. Immunomodulation by therapeutic mesenchymal stromal cells (msc) is triggered through phagocytosis of msc by monocytic cells. *Stem Cells*, 36(14):602–615, 2018. doi: <https://doi.org/10.1002/stem.2779>. URL <https://pubmed.ncbi.nlm.nih.gov/29341339/>.
- M. Dominici, K. L. Blanc, I. Mueller, I. Slaper-Cortenback, F. C. Marini, D. Krause, R. J. Deans, A. Keating, D. J. Prockop, and E. M. Horwitz. Minimal criteria for defining multipotent mesenchymal stromal cells. the international society for cellular therapy position statement. *Cytotherapy*, 8(4):315–317, 2006. doi: <https://doi.org/10.1080/14653240600855905>. URL <https://pubmed.ncbi.nlm.nih.gov/16923606/>.
- J. M. Gimble and F. Guilak. Adipose-derived adult stem cells: isolation, characterization, and differentiation potential. *Cytotherapy*, 5(5):362–369, 2003. doi: 10.1080/14653240310003026. URL <https://pubmed.ncbi.nlm.nih.gov/14578098/>.
- R. Guillamat-Prats. The role of msc in wound healing, scarring and regeneration. *Cells*, 10(7):1729, 2021. doi: 10.3390/cells10071729. URL <https://www.mdpi.com/2073-4409/10/7/1729>.
- S. B. Hansen, L. D. Højgaard, J. Kastrup, A. Ekblond, B. Follin, and M. Juhl. Optimizing an immunomodulatory potency assay for mesenchymal stromal cell. *Frontiers in Immunology*, 13:1–12, 2022. doi: <https://doi.org/10.3389/fimmu.2022.1085312>. URL <https://www.frontiersin.org/articles/10.3389/fimmu.2022.1085312/full>.

- L. Hidalgo-Garcia, J. Galvez, M. E. Rodriguez-Cabezas, and P. O. Anderson. Can a conversation between mesenchymal stromal cells and macrophages solve the crisis in the inflamed intestine? *Front Pharmacol*, 9:179, 2018. doi: 10.3389/fphar.2018.00179. URL <https://www.ncbi.nlm.nih.gov/pmc/articles/PMC5845680/>.
- M. Holthaus, N. Santhakumar, T. Wahlers, and A. Paunel-Görgülü. The secretome of preconditioned mesenchymal stem cells drives polarization and reprogramming of m2a macrophages toward an il-10-producing phenotype. *International Journal of Molecular Sciences*, 23(8):4104, 2022. doi: <https://doi.org/10.3390/ijms23084104>. URL <https://pubmed.ncbi.nlm.nih.gov/35456922/>.
- M. Jaguin, N. Houlbert, O. Fardel, and V. Lecureur. Polarization profiles of human m-csf-generated macrophages and comparison of m1-markers in classically activated macrophages from gm-csf and m-csf origin. *Cellular Immunology*, 281(1):51–61, 2013. doi: <https://doi.org/10.1016/j.cellimm.2013.01.010>. URL <https://www.sciencedirect.com/science/article/pii/S0008874913000233>.
- R. T. Kendall and C. A. Feghali-Bostwick. Fibroblasts in fibrosis: novel roles and mediators. *Front Pharmacol*, 5(123), 2014. doi: 10.3389/fphar.2014.00123. URL <https://www.frontiersin.org/articles/10.3389/fphar.2014.00123/full>.
- P. Luz-Crawford, C. Jorgensen, and F. Djouad. Mesenchymal stem cells direct the immunological fate of macrophages. *Results and Problems in Cell Differentiation*, 62:61–72, 2017. doi: [https://doi.org/10.1007/978-3-319-54090-0\\_4](https://doi.org/10.1007/978-3-319-54090-0_4). URL <https://pubmed.ncbi.nlm.nih.gov/28455706/>.
- R. Myllylä and H. Seppä. Studies on enzymes of collagen biosynthesis and the synthesis of hydroxyproline in macrophages and mast cells. *Biochem J*, 182(2):311–316, 1979. doi: <https://doi.org/10.1042/bj1820311>. URL <https://pubmed.ncbi.nlm.nih.gov/228650/>.
- M. Schnoor, P. Cullen, J. Lorkowski, K. Stolle, H. Robenek, D. Troyer, J. Rauterberg, and S. Lorkowski. Production of type vi collagen by human macrophages: a new dimension in macrophage functional heterogeneity. *J immunol*, 180(8):5707–5719, 2008. doi: <https://doi.org/10.4049/jimmunol.180.8.5707>. URL <https://pubmed.ncbi.nlm.nih.gov/18390756/>.
- E. Setten, A. Castagna, J. M. Nava-Sedeño, J. Weber, R. Carriero, A. Reppas, V. Volk, J. Schmitz, W. Gwinner, H. Hatzikirou, F. Feuerhake, and M. Locati. Understanding fibrosis pathogenesis via modeling macrophage-fibroblast interplay in immune-metabolic context. *Nat Commun*, 13(1):6499, 2022. doi: 10.1038/s41467-022-34241-5. URL <https://www.nature.com/articles/s41467-022-34241-5>.
- A. Shapouri-Moghaddam, S. Mohammadian, H. Vazini, M. Taghadosi, S. Esmaili, F. Mardani, B. Seifi, A. Mohammadi, J. T. Afshari, and A. Sahebkar. Macrophage plasticity,

- polarization, and function in health and disease. *Journal of Cellular Physiology*, 233(9): 6425–6440, 2018. doi: 10.1002/jcp.26429. URL <https://pubmed.ncbi.nlm.nih.gov/29319160/>.
- H. Y. Stevens, A. Bowles, C. Yeago, and K. Roy. Molecular crosstalk between macrophages and mesenchymal stromal cells. *Front Cell Dev Biol.*, 8:600160, 2020. doi: 10.3389/fcell.2020.600160. URL <https://www.ncbi.nlm.nih.gov/pmc/articles/PMC7755599/>.
- R. H. Søndergaard, L. D. Højgaard, A. L. Reese-Petersen, C. Hoeg, A. B. Mathiasen, M. H. Sørensen, B. Follin, F. Genovese, J. Kastrup, M. Juhl, and A. Ekblond. Adipose-derived stromal cells increase the formation of collagens through paracrine and juxtacrine mechanisms in a fibroblast co-culture model utilizing macromolecular crowding. *Stem Cell Research and Therapy*, 13:250, 2022. doi: <https://doi.org/10.1186/s13287-022-02923-y>. URL <https://stemcellres.biomedcentral.com/articles/10.1186/s13287-022-02923-y>.
- I. Ushach and A. Zlotnik. Biological role of granulocyte macrophage colony-stimulating factor (gm-csf) and macrophage colony-stimulating factor (m-csf) on cells of the myeloid lineage. *Journal of Leukocyte Biology*, 100(3):481–489, 2016. doi: 10.1189/jlb.3RU0316-144R. URL <https://www.ncbi.nlm.nih.gov/pmc/articles/PMC4982611/>.
- G. F. Vasse, M. Nizamoglu, I. H. Heijink, M. Schlepütz, P. V. Rijn, M. J. Thomas, J. K. Burgess, and B. N. Melgert. Macrophage–stroma interactions in fibrosis: biochemical, biophysical, and cellular perspectives. *The Journal of Pathology*, 254(4):344–357, 2021. doi: 10.1002/path.5632. URL <https://www.ncbi.nlm.nih.gov/pmc/articles/PMC8252758/>.
- World Medical Association. World medical association declaration of helsinki. ethical principles for medical research involving human subjects. *Bulletin of the World Health Organization*, 79(4):373–374, 2001. doi: <https://apps.who.int/iris/handle/10665/268312>.
- S. Zhang, Q. Huang, X. Cai, S. Jiang, N. Xu, Q. Zhou, X. Cao, M. Hulström, J. Tian, and E. Y. Lan. Osthole ameliorates renal fibrosis in mice by suppressing fibroblast activation and epithelial-mesenchymal transition. *Frontiers in Physiology*, 9:1650, 2018. doi: 10.3389/fphys.2018.01650. URL <https://www.ncbi.nlm.nih.gov/pmc/articles/PMC6258720/>.
- X. Zhao, J. Chen, H. Sun, Y. Zhang, and D. Zou. New insights into fibrosis from the ecm degradation perspective: the macrophage-mmp-ecm interaction. *Cell & Bioscience*, 177, 2022. doi: <https://doi.org/10.1186/s13578-022-00856-w>. URL <https://pubmed.ncbi.nlm.nih.gov/35897082/>.
- G. Zhou, H. Loppnow, and T. Groth. A macrophage/fibroblast co-culture system using a cell migration chamber to study inflammatory effects of biomaterials. *Acta Biomaterialia*, 26:54–63, 2015. doi: <https://doi.org/10.1016/j.actbio.2015.08.020>. URL <https://pubmed.ncbi.nlm.nih.gov/26292266/>.

# A | Appendix

## A.1 Table of Macrophage Markers

	Shared	Immature	Mature	
			M1 macrophages	M2 macrophages
<b>Stimulating Factors</b>	-	-	IFN- $\gamma$ TNF- $\alpha$ LPS	IL-4 IL-13
<b>Markers</b>	HLA-DR CD80 CD86	CD14	CD40 TLR4	CD206
<b>Secretome</b>	-	TNF- $\alpha$ IL-6 IL-12 CXCL9 CXCL10	TNF- $\alpha$ IL-1 IL-6 IL-12 ROS	TGF- $\beta$ IL-10 IL-1-RA CCL17 CCL22

**Simplified overview of macrophage markers.** The macrophage markers as well as their secretome differ based on both their activational and polarisation state. IFN- $\gamma$ : interferon- $\gamma$ , TNF- $\alpha$ : tumor necrosis factor- $\alpha$ , LPS: lipopolysaccharide, IL: interleukin, HLA: human leukocyte antigen, TLR: Toll-like receptor, CXCL: C-X-C motif chemokine ligand, ROS: reactive oxygen species, IL-1-RA: IL-1 receptor antagonist, CCL: C-C Motif Chemokine Ligand.

## A.2 Dilution of Samples for ELISA

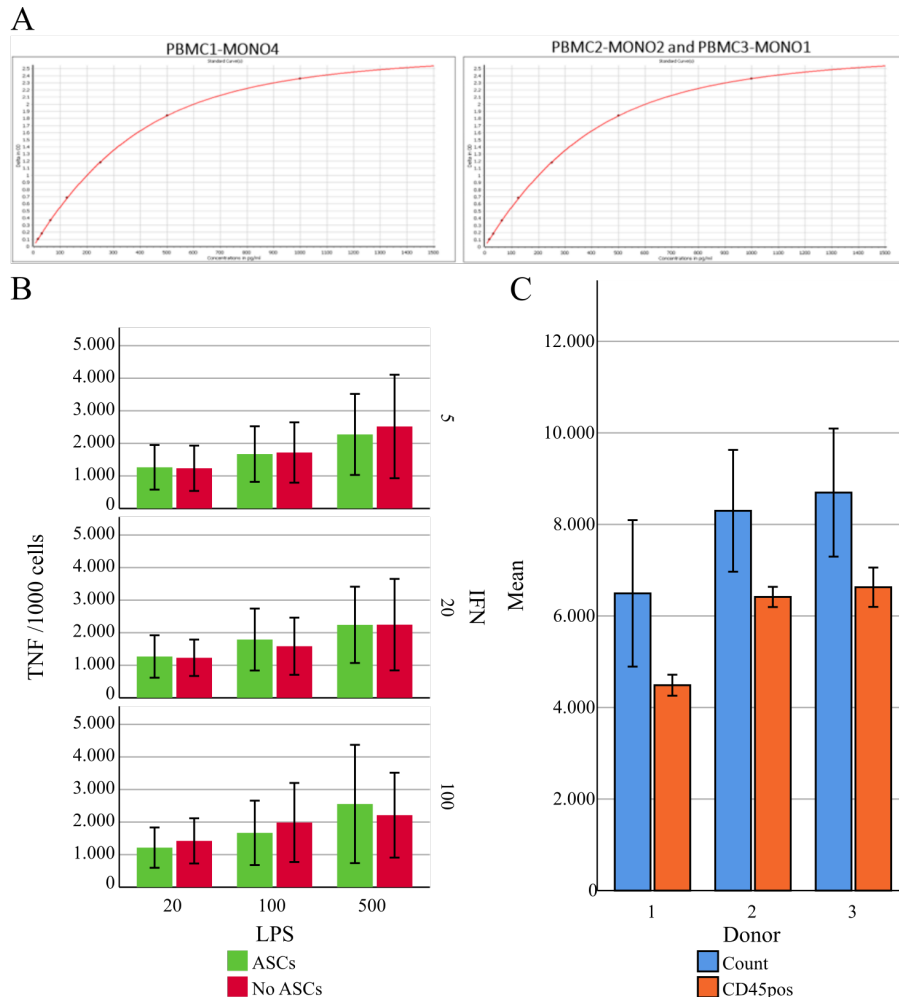
5-Parameter fit based on Difference in pg/ml (calculated)								
	1	2	3	4	5	6	7	8
A	892.253	549.042	218.123	123.101	65.665	31.157	15.251	n.a.
B	992.368	592.208	243.674	126.889	61.075	31.522	15.897	n.a.
C	>> std. range	>> std. range	778.911	854.608	105.68	104.743	14.185	13.767
D	>> std. range	>> std. range	>> std. range	>> std. range	801.831	808.042	79.653	75.166
E	>> std. range	>> std. range	1380.27	1285.148	334.565	355.738	38.123	37.349

	Range of Standards
	PBMC-1 MONO-4
	PBMC-2 MONO-2
	PBMC-3 MONO-1
1x	Row 1-2
5x	Row 3-4
25x	Row 5-6
125x	Row 7-8

**Dilution of samples for ELISA.** OMEGA Mars Software was used for data analysis of ELISA readings from the plate reader. The Range of Standard was corrected with a 5-parameter fit with R<sup>2</sup> at 99.9%. Donor 1: PBMC1, Donor 2: PBMC2, Donor 3: PBMC3. PBMC: peripheral blood mononuclear cell.

### A.3 Determination of Optimal Concentrations of Activating Stimuli



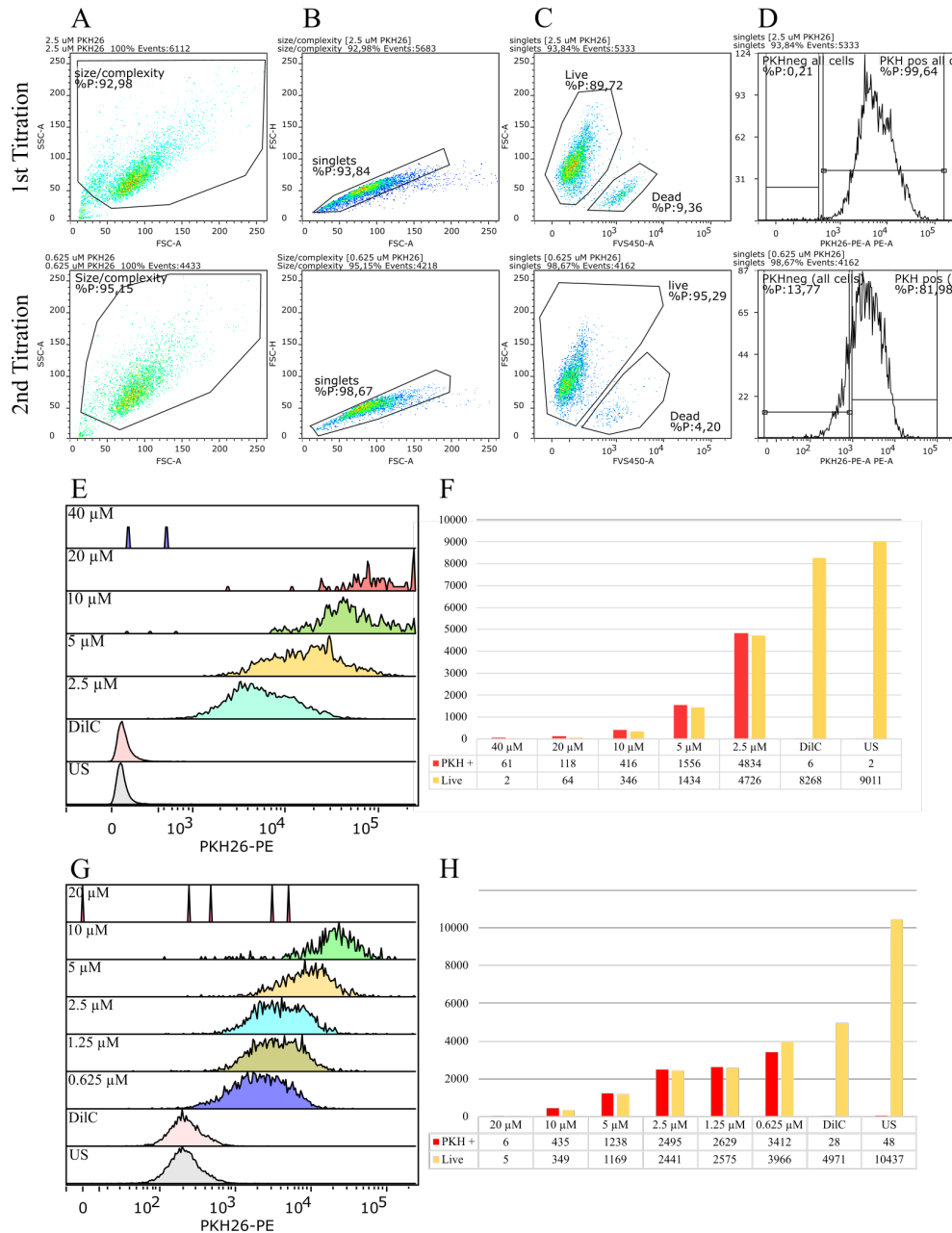
**Determination of TNF- $\alpha$  concentration.** A: Standard Curves for analysis of samples. OMEGA Mars Software was used for data analysis of ELISA readings from the plate reader. Standard curve was corrected with a 5-parameter fit based on range of standards with  $R^2=99.9\%$ . B: TNF- $\alpha$  concentration in pg/mL per 1000 cells by concentration of LPS and IFN- $\gamma$  in ng/mL. Error bars indicate  $\pm 1$  standard deviation. C: Mean cell count based on Hoechst staining (blue) and CD45 staining (red). The concentration of TNF was normalised based on staining with CD45 and Hoechst. Macrophages were labelled with CD45 and all nuclei were stained with Hoechst. Differences in cell count between CD45 and Hoechst account for the number of ASCs. Donor 1: PBMC1, Donor 2: PBMC2, Donor 3: PBMC3. ASC: adipose-derived stromal cell; tumor necrosis factor- $\alpha$ , LPS: lipopolysaccharide, IFN: interferon- $\gamma$ .

## A.4 Channels in Fluorescent Microscopy

Method	Channel	Filter Set
Hoechst 33342	DAPI	1
Sirius Red in Picrin Acid	AF546	43
Rabbit anti-mouse IgG (H+L)	AF555	43
Goat anti-mouse IgG	AF488	38
Goat anti-rabbit IgG (H+L)	AF546	43

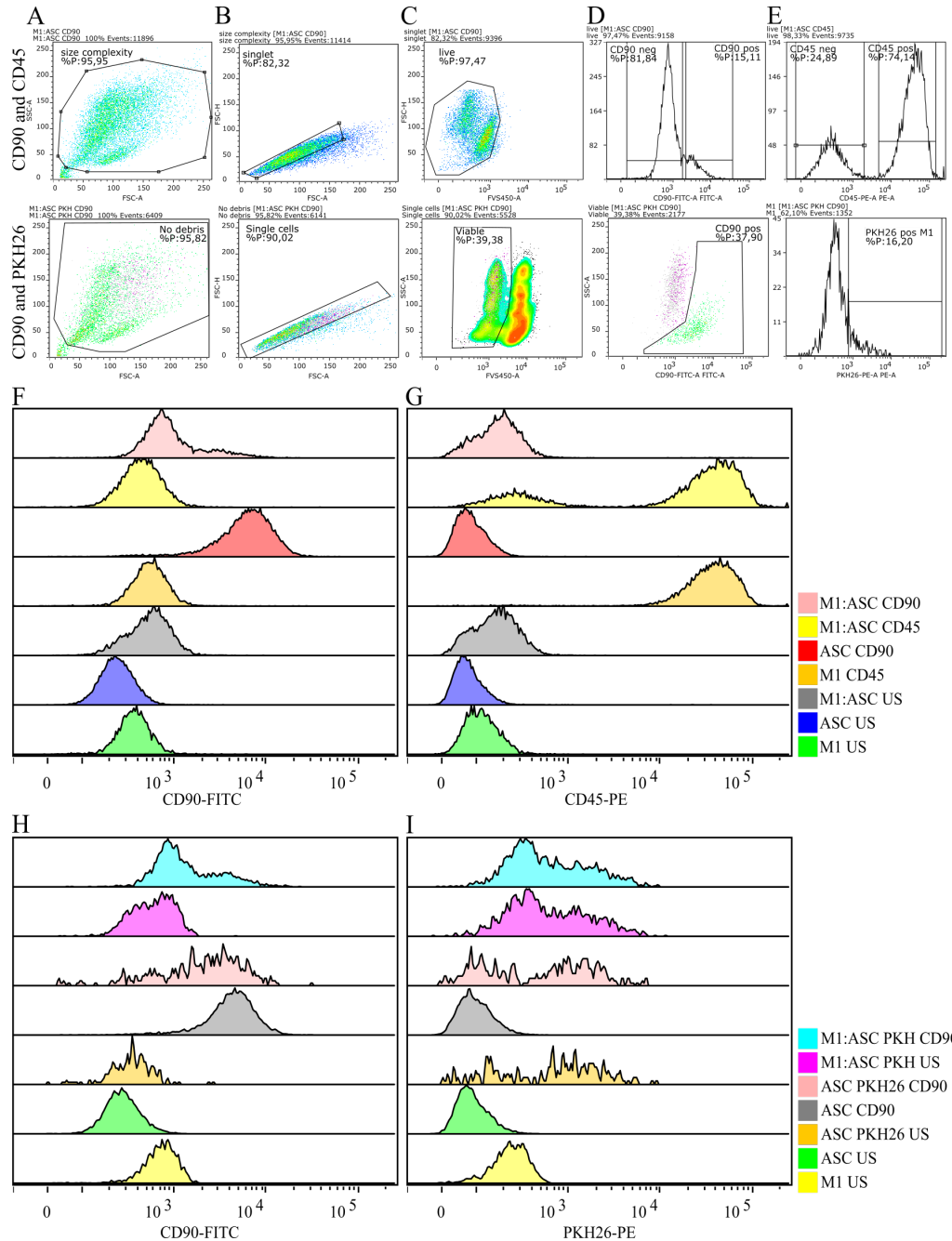
**Channels in Fluorescent Microscopy.** Depending on the use of secondary antibodies, Hoechst or PicroSirius separate channels were acquired during fluorescent microscopy. The filter set numbers refer to those defined by Zeiss Microscopy. AF: alexa fluor, IgG: immunoglobulin G, H+L: heavy and light chain.

## A.5 Optimization of PKH26 Concentration



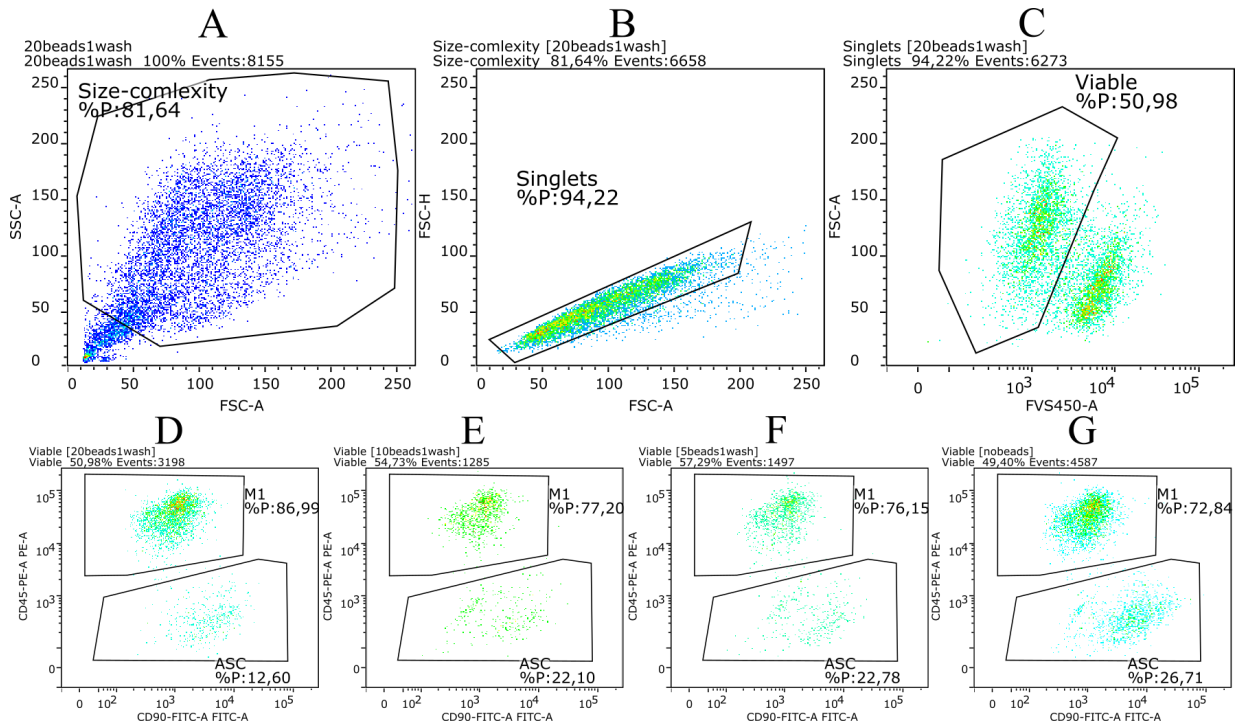
**Optimization of PKH26 concentration.** Gating strategy for PKH26 flow cytometry data. A: Gating to remove debris. B: Gating to remove doublets. C: Gating for live cells. D: Gating for PKH26-positive cells based on singlets. E: Overlay of PKH26 intensity of live cells from the first titration. F: Number of PKH26-positive cells (PKH +) in relation to the number of live cells (Live) in the first titration. G: Overlay of PKH26 intensity of live cells from the second titration. H: Number of PKH26-positive cells (PKH +) in relation to the number of live cells (Live) in the second titration. Labels on the overlays indicate the concentration of PKH26. DilC: Diluent C Control, US: Unstained Control.

## A.6 Flowcytometric Analysis using CD45 and CD90



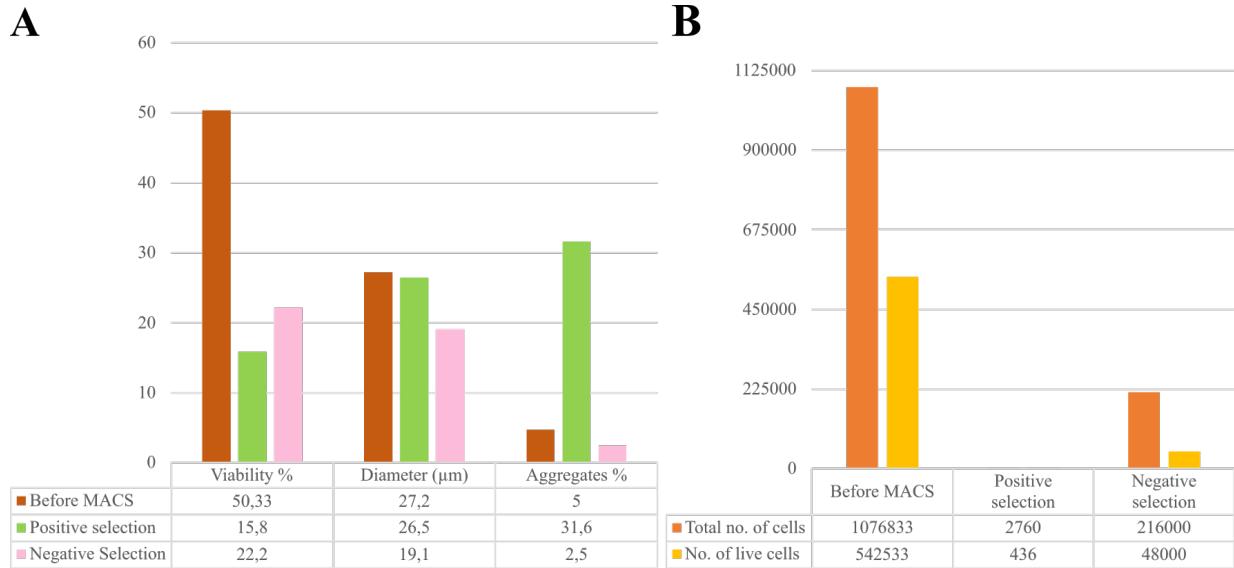
**Flow cytometry analysis using CD45 and CD90.** A: Gating to remove debris. B: Gating to remove doublets. C: Gating for live cells. D: Gating for CD90-positive cells. E, top picture: Gating for CD45-positive cells. E, bottom picture: Boolean gating for isolation of the M1 population of the viable cells by excluding CD90-positive cells. F: Overlay of CD90-positive live cells. G: Overlay of CD45-positive live cells. H: Overlay of CD90-positive live cells. I: Overlay of the PKH26-positive live cells. US: Unstained Control. PKH: PKH26 membrane stain.

## A.7 Titration of Dynabeads



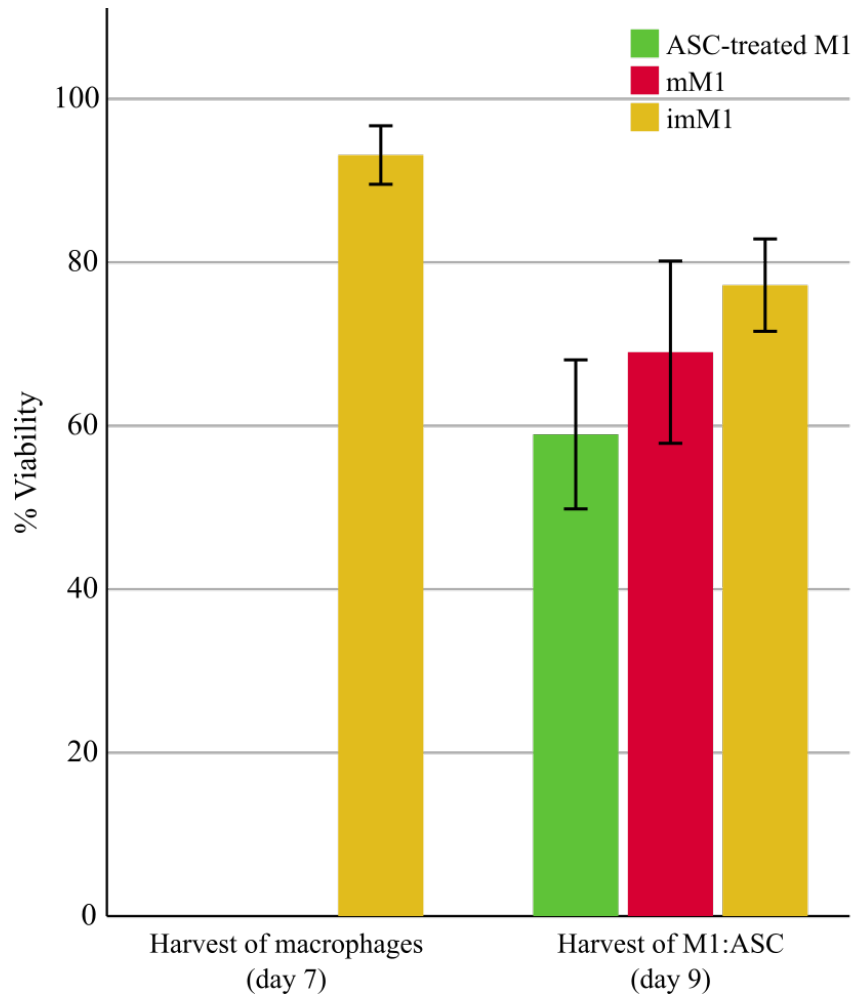
**Titration of Dynabeads.** A: Gating to remove debris. B: Gating to remove doublets. C: Gating for live cells. D: When using 20 beads/cell there are 12.6% ASCs left. E: With 10 beads/cell there are 22.1% ASCs left. F: With 5 beads/cell there are 22.8% ASCs left. G: In the control without beads there are 26.7% ASCs left. ASC: Adipose Tissue-derived Stromal Cell.

## A.8 Aggregation in a Single Cell Suspension



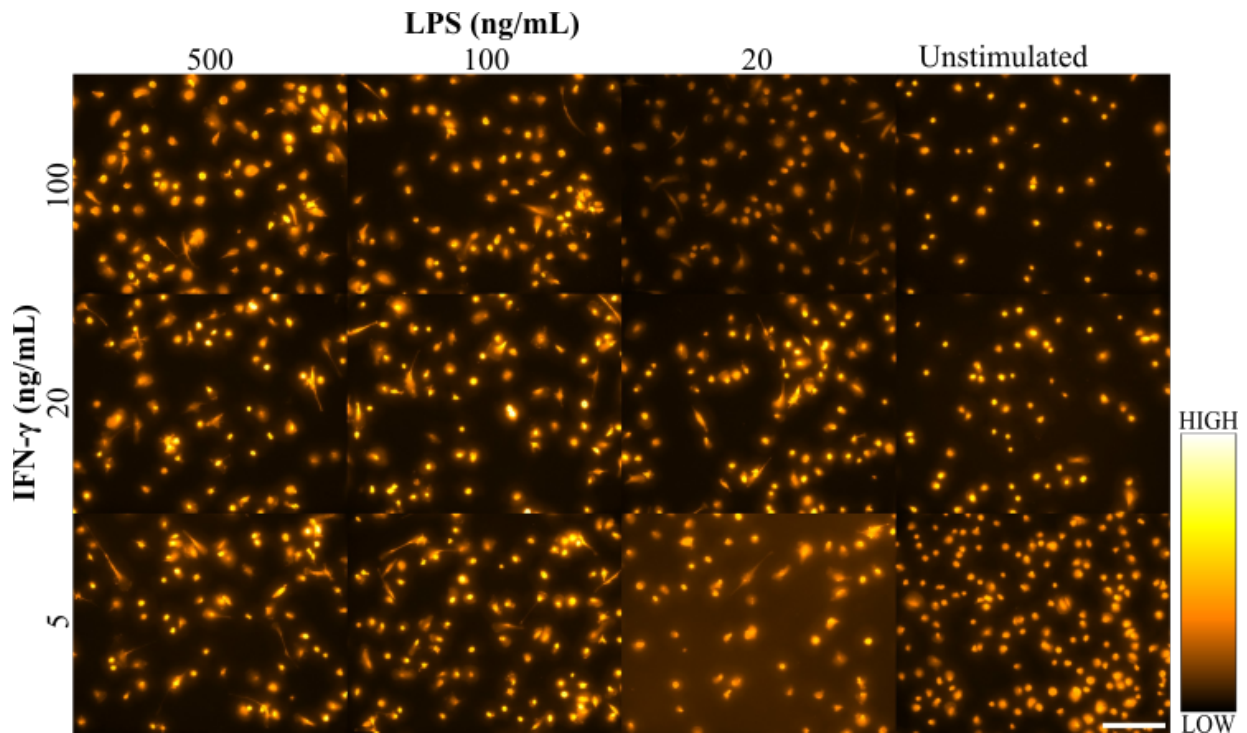
**Assesment of Single Cell Suspension A:** Comparison of cell viability and aggregation (in percentage) to the cell diameter ( $\mu\text{m}$ ). **B:** Total number of cells and live number of cells in the positive and negative selection after sorting with magnetic-activated cell sorting compared to an unsorted sample.

## A.9 Macrophage Viability



**Macrophage viability after harvest on day seven and nine.** Macrophage viability in percentage after harvesting on day six prior to macrophage-ASC-coculture, compared to day nine after harvest of macrophage-ASC-coculture. Error bars indicate  $\pm 1$  standard deviation. ASC: Adipose-derived stromal cell, mM1: mature M1 macrophage, imM1: immature M1 macrophage. M1:ASC: macrophage-ASC-coculture

## A.10 PicroSirius Staining of Macrophages



**PicroSirius staining of macrophages.** To illustrate the amount of unspecific staining, macrophages were stimulated with different concentrations of LPS and IFN- $\gamma$  and stained with PicroSirius. Brightness and contrast is fixed for all images. Scale 200  $\mu\text{m}$ . LPS: lipopolysaccharide, IFN- $\gamma$ : interferon- $\gamma$ .